Fluorescence Micro-spectroscopy Assessment of the in vitro Dimerization of BACE1-GFP Fusion Protein in Cultured Cells

A THESIS
SUBMITTED TO THE FACULTY OF
UNIVERSITY OF MINNESOTA
BY

Spencer Gardeen

IN PARTIAL FULFILLMENT OF THE REQUIREMENTS
FOR THE DEGREE OF
MASTER OF SCIENCE

Thesis Advisors:
Dr. Joseph L. Johnson, Dr. Ahmed Heikal

November 2015

Acknowledgements

I would like to thank Dr. Bradley Hyman for his generous gift of BACE1-EGFP construct and Dr. Lynne Bemis (Medical School, University of Minnesota Duluth*; Department of Biomedical Sciences*) for her gift of a flask of HEK293 cells. In addition I would like to thank my committee members Dr. Steven Berry and Dr. Erin Sheets for their time and commitment to my thesis project. Most of all, I would like to acknowledge Dr. Heikal and Dr. Johnson for the countless hours and tireless effort they have put into helping me learn and setup my project. Without them I would not be the same person I am today.

Dedication

This thesis is dedicated to my loving family, who has always supported me in my scientific endeavors and pursuit of knowledge.

Abstract

Alzheimer's Disease (AD) is a neurodegenerative disorder that results from the formation of beta-amyloid (Aβ) plaques in the brain, which according to the amyloid cascade hypothesis triggers known symptoms, such as memory loss, in AD patients. Aβ plaques are formed by the proteolytic cleavage of the amyloid precursor protein (APP) by the proteases BACE1 and γ-secretase. These enzyme-facilitated cleavages lead to the production of Aβ fragments that then aggregate to form plaques, which ultimately lead to neuronal cell death. Recent detergent protein extraction studies suggest that the untreated BACE1 protein forms a dimer that has significantly higher catalytic activity than its monomeric counterpart. Currently, however, there are no studies that support the dimerization hypothesis of BACE1 in living cells. In this contribution, we describe our effort to examine the dimerization hypothesis of BACE1 in cultured HEK293 cells using complementary fluorescence spectroscopy and microscopy methods. Cells were transfected with a BACE1-EGFP fusion protein construct and imaged using confocal and differential interference contrast (DIC) microscopy to monitor labeled BACE1 localization and distribution within the cell. Subsequently, single molecule fluctuation analysis allowed us to test the dimerization hypothesis of the labeled BACE1 using fluorescence measurements of the diffusion coefficient (size-dependent observable) and the molecular brightness as a function of BACE1 substrate analog inhibitor binding. Complementary two-photon fluorescence lifetime and anisotropy imaging enabled us to monitor BACE1 conformational changes and its local environment as a function of

substrate binding. These studies provide evidence that BACE1 substrate-mediated dimerization occurs in cells and may be dependent on cellular location.

Table of Contents

List of Tables

List of Figures

List of Abbreviations

Aβ	Amyloid Beta
AD	Alzheimer's disease
APP	Amyloid Precursor Protein
AICD	APP intracellular domain
BACE1	β-Site Amyloid Precursor Cleaving Enzyme-1
DIC	Differential Interference Contrast
EMEM	Eagle's Minimum Essential Medium
EGFP	Enhanced Green Fluorescent Protein
ER	Endoplasmic Reticulum
FBS	Fetal Bovine Serum
FCS	Fluorescence Correlation Spectroscopy
FLIM	Fluorescence Lifetime Imaging Microscopy
FRET	Fluorescence Resonance Energy Transfer
FWHM	Full-Width Half-Maximum
GGA	γ-ear-containing ARF-binding
HEK	Human Embryonic Kidney
IC	Internal Compartment
NA	Numerical Aperture
1P	One-Photon
PBS	Phosphate Buffered Saline
PM	Plasma Membrane
RhG	Rhodamine Green
2P	Two-Photon
TGN	Trans-Golgi Network
trFA	Time-Resolved Fluorescence Anisotropy

List of Symbols

χ^2	Chi-Squared
t	Time
τ	Correlation Lag Time
f	Fraction
β	Amplitude in Anisotropy Decay
ϕ	Rotational Time
η	Viscosity
V	Hydrodynamic Volume
k_B	Boltzmann Constant
T	Temperature
D	Diffusion Coefficient
D_T	Translational Diffusion Coefficient
D_R	Rotational Diffusion Coefficient
I	Fluorescence Intensity
$r(t)$	Anisotropy
a	Hydrodynamic Radius
π	Pi
C	Concentration
∇	Gradient
δI	Fluorescence Fluctuation
N	Number
ω_{xy}	Lateral Extension of the Observation Volume in FCS
h	Degree of Hydration of a Protein
E	Energy Transfer Efficiency
R_{DA}	Donor-Acceptor Distance
R_0	Förster distance between Donor and Acceptor at which E=50%
$J(\lambda)$	Spectral Overlap
Φ	Fluorescence Quantum Yield
τ_{fl}	Excited-State Fluorescence Lifetime
τ_{DA}	Fluorescence Lifetime of Donor-Acceptor Pair
τ_D	Fluorescence Lifetime of a Donor alone (no Acceptor)
y	Mean

σ	Standard Deviation
K	Kelvin
°C	Degrees Celsius

Chapter 1

Introduction

1.1 BACE1 Discovery and Amyloid Beta Hypothesis in Alzheimer's Disease

First characterized by Alois Alzheimer in 1906, Alzheimer's disease (AD) is a neurodegenerative disorder that leads to progressive memory loss and ultimately to death.[1] Currently 5.3 million people in the United States alone live with AD, and this number is expected to rise to 16 million by the year 2050.[1] Not only will this rise in the number of Alzheimer's patients directly affect the lives of millions, but it is also projected to put a great financial strain on society by increasing the cost of the patient care from $226 billion to an astonishing $1.1 trillion.[1] AD remains the only top ten cause of death in America that cannot be slowed significantly, prevented, or cured.[1] It is for these reasons that the study of AD is of the utmost importance.

One hallmark of AD is the formation of amyloid plaques. These amyloid plaques consist primarily of aggregated amyloid beta (Aβ), which results from the processing of the amyloid precursor protein (APP) by a series of proteolytic (or secretase) activities.[2] APP is a type I membrane protein (single transmembrane domain with the C-terminus on the cytoplasmic face of the lipid bilayer) that is involved in a multitude of native cellular processes including neuronal migration, signal transduction, and transport of a variety of proteins.[3,4] Figure 1.1 depicts the two predominant pathways in which APP is processed to either produce Aβ or non-pathogenic peptide fragments, which are referred to as amyloidogenic and non-amyloidogenic, respectively. In the amyloidogenic pathway, APP

is first cleaved by β-secretase (BACE1 in Figure 1.1), which is the rate limiting activity for Aβ formation, to produce a soluble fragment (s-APPβ) and a membrane bound fragment (C99).[5,6] C99 is then cleaved within the lipid bilayer by γ-secretase to produce the APP intracellular domain (AICD) and either Aβ-40 or -42.[7,8] The amyloid beta peptide fragments combine to form oligomers, which then aggregate to generate fibrils that further condense to form plaques.[9,10] Some of the intermediates along the pathway towards Aβ plaque formation have been shown to be responsible for aberrant effects such as disruption of cell signaling, formation of tangles composed of aggregates of the hyperphosphorylated protein tau, and elicitation of an immune response that ultimately leads to cell death and reduced brain mass.[11-14] Alternatively, APP can be cleaved by α-secretase to produce a soluble fragment (s-APPα) and C83.[15] C83 is then cleaved by γ-secretase to yield the non-pathogenic protein fragments P3 and AICD.[16]

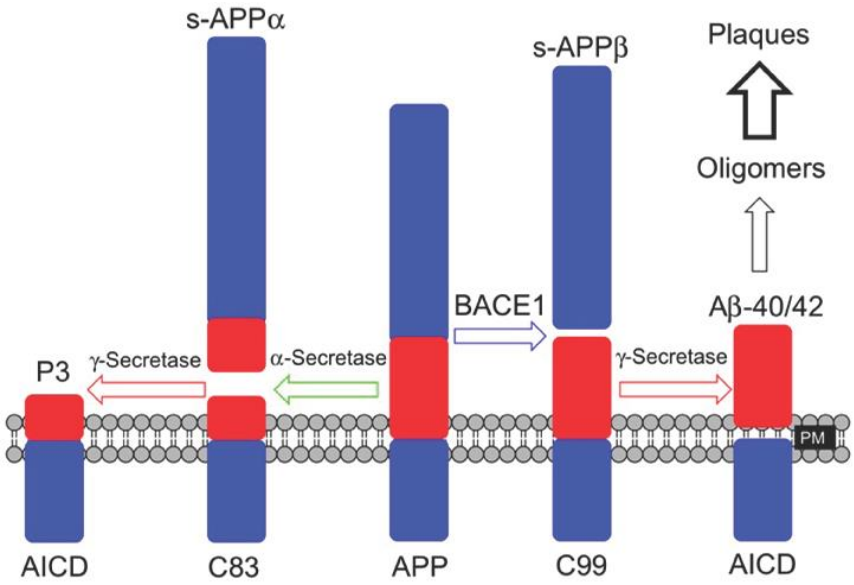

Figure 1.1: Non-amyloidogenic and Amyloidogenic Processing of APP.

Starting in 1987 research showed that Aβ production was a direct result of cleavage of APP by two distinct activities, specifically β-secretase and γ-secretase activities. However, it would take another twelve years of research to identify the protein responsible for the β-secretase activity.[4,17] BACE1 (or beta-site APP cleaving enzyme 1) was co-discovered by five independent research groups over a short period of time: Yan *et al.*, Sinha *et al.*, Hussain *et al.*, Lin *et al.*, and Vassar *et al.* in 1999.[17-22] The groups of Lin, Yan, and Hussain applied strategies that required assessing genomic data from a variety of species and making biochemical deductions as to which sequences would most likely be responsible for the observed β-secretase activity.[17,18,20-22] These candidates were then transfected into cells and screened for β-secretase activity.[18,20,21] Vassar *et al.* screened large pools of cDNA for β-secretase activity using ELISA assays to monitor Aβ levels and continually subdividing the pools until the lone remaining gene was isolated

and identified as BACE1.[22] Sinha *et al.* utilized affinity chromatography with a peptide transition state analog attached to NHS-sepharose.[19] After isolation, the protein sequence was determined, and the group constructed the appropriate cDNA.[19]

Throughout this thesis the term BACE1 will be used, but it also has other commonly accepted names in the literature such as Asp 2 (novel aspartic protease 2) and memapsin-2 (membrane aspartic protease/pepsin 2). This assortment of names for the same protein arose from its simultaneous discovery by a variety of research groups.

1.2 Biosynthesis, Modification and Cellular Trafficking of BACE1

BACE1 is first synthesized as a pro-peptide in endoplasmic reticulum (ER) where it is N-glycosylated at four asparagine residues 153, 172, 223, and 354.[23] To help stabilize BACE1 as well as facilitate its transport to the trans-Golgi network (TGN), it is acetylated seven times at seven different lysine residues within the ER.[24] After completion of all the modifications in the ER, BACE1 is trafficked to the TGN where the acetylated lysine residues are deacetylated.[24] Once in the TGN, the 45 amino acid long prodomain of BACE1 is removed by the protease furin and the resulting protein is palmitoylated at 474, 478, 482, and 485 to produce the fully mature protein.[25] These palmitoylations are thought to be responsible for the association of BACE1 with lipid rafts on the plasma membrane.[26]

Following post-translational modifications in the TGN, BACE1 is transported to the cell membrane where it is then internalized via clathrin-coated pits into early

endosomes by interacting with ADP ribosylation factor 6 (ARF6).[27,28] Once in the early endosome, BACE1 activity increases due to the lower pH of the compartment facilitating acid-base cleavage of peptide substrates.[16,22] Following cleavage of substrate, regulation due to phosphorylation of Ser-498 within the C-terminal domain of BACE1 can cause it to interact with Golgi-localized γ-ear-containing ARF-binding 1 (GGA1) protein resulting in transport back to the plasma membrane through recycling endosomes and the TGN.[29] Alternatively, mono-ubiquitination of BACE1 and interactions with GGA3 target it to lysosomes for degradation.[30] This process of BACE1 cellular trafficking is highlighted in Figure 1.2.

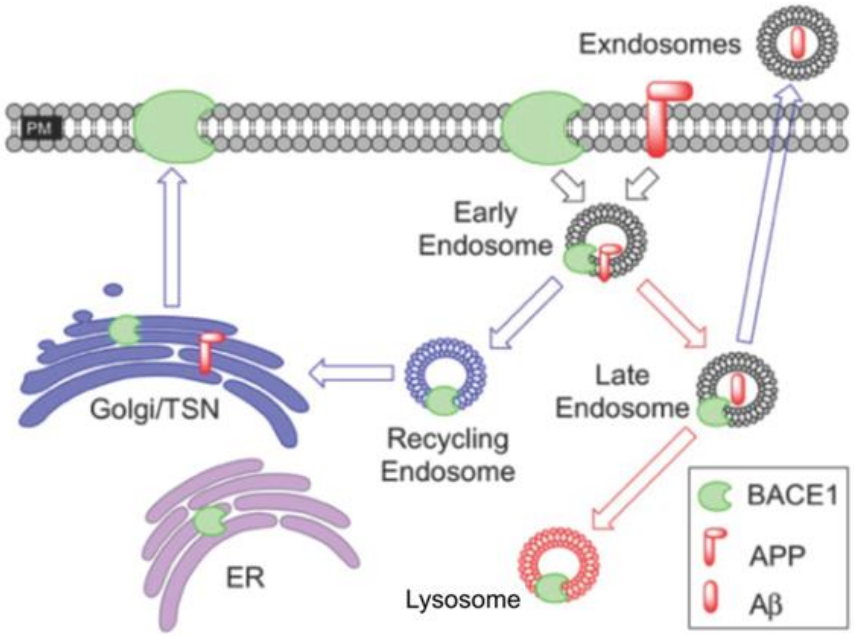

Figure 1.2: Cellular Trafficking of BACE1. Representative scheme depicting BACE1 localization within different cellular compartments. BACE1 is first synthesized in the ER where it is glycosylated and acetylated. It is then trafficked to the TGN where it is deacetylated and palmitoylated, after which BACE1 is sent to the plasma membrane where it undergoes endocytosis into early endosomes. Following substrate cleavage, BACE1 can either be recycled back to the plasma membrane or sent to lysosomes for degradation.

1.3 Beta-site APP Cleaving Enzyme (BACE1) Structure-Function Relationship

BACE1 is a type I transmembrane aspartyl protease composed of 501 amino acids consisting of three structural domains with a total molecular weight of approximately ~75 kDa when fully matured.[18-22] The three domains of this pepsin-like aspartyl protease are shown in Figure 1.3A: the N-terminal extracellular catalytic domain, the single-pass α-helical transmembrane domain, and the small C-terminal cytosolic domain.

The extracellular domain, which is folded into two lobes forming a furrowed central cleft, is responsible for binding and subsequent acid-base cleavage of the scissile peptide bond of the bound protein substrate (Figure 1.4).[31] The binding cleft is made up of eleven subsites (P1-P7 and P1′-P4′) flanking the catalytic aspartyl dyad.[31,32] These subsites interact with specific substrate amino acids to facilitate binding and subsequent cleavage of peptide substrates.[31,32] The extracellular domain is homologous to that of pepsin including a β-hairpin "flap" that protects the active site but, in addition, it also has four well-defined insertions forming loops A, C, D, and F, the functions of which have yet to be elucidated.[33]

The single-pass α-helical transmembrane domain of BACE1 is a series of hydrophobic residues, including several methionine and cysteine residues which have been shown to possess the ability to chelate to copper ions using model peptides *in vitro*.[33] This transmembrane domain acts as an anchor, restricting movement of the protease to cellular membranes. In addition, BACE1 has been modeled and shown to spontaneously oligomerize under artificial conditions.[32]

The C-terminal domain of BACE1 is a small (~5 kDa) segment extending into the cytoplasm.[27] Although it is small relative to the rest of the protein, the C-terminal domain of BACE1 is crucial for cellular trafficking. Three key residues (Ser498, Leu499, and Leu500) regulate transport from the cell membrane to early endosomes as well as recycling and degradation of BACE1 by interaction with GGA proteins.[27-30]

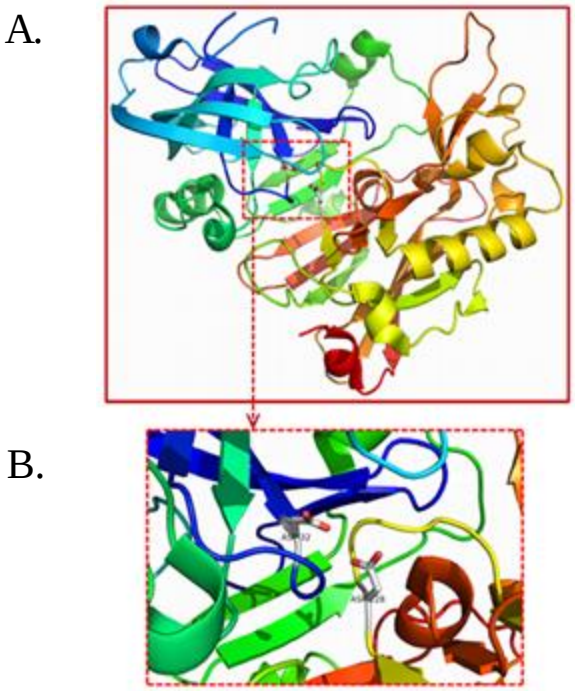

Figure 1.3: Crystal Structure Representations of BACE1. Panel A: Crystal structure of BACE1 catalytic domain (PDB:1FKN). Panel B: Zoomed in view of the catalytic aspartate residues.

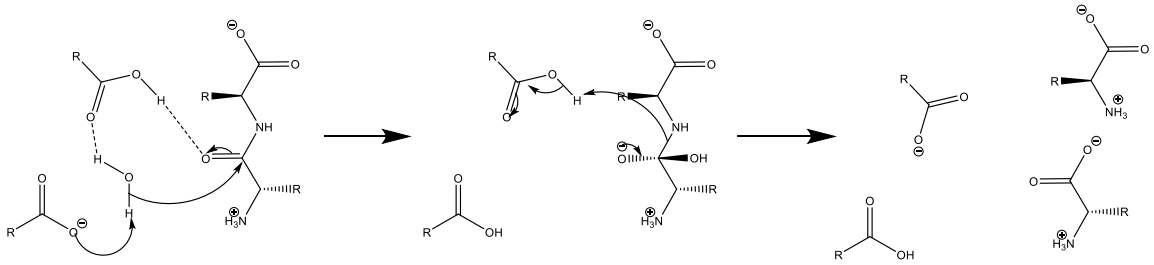

Figure 1.4: Generic Aspartyl Protease Mechanism. Diagram shows the backbone cleaving mechanism carried out by the activation of a water molecule by the aspartic dyad.

1.4 BACE1 Dimerization Hypothesis: Existing Evidences and Challenges

In 2004 two reports were published that provided evidence suggesting that BACE1 forms constitutive dimers.[34,35] The first included work done by the Haass group providing novel evidence of BACE1 dimers extracted using detergents and strong denaturing conditions from brains of Alzheimer's disease patients.[34] In this study the researchers provided evidence of BACE1 dimerization through common biochemical techniques such as SDS-PAGE and Western blotting. In addition, they showed that by transfecting cells with two populations of complementary BACE1 active site aspartyl mutants they were able to achieve successful dimerization and production of s-APPβ as well as Aβ.[34] It was also shown that BACE1 and the BACE1 mutants co-localized with APP using immunoelectron microscopy and immunofluorescence.[34]

The second paper from the Haass group also provided three key pieces of evidence pertaining to BACE1 dimerization that are worth mentioning.[35] A Western blot was generated using blue native polyacrylamide gel electrophoresis (BN-PAGE), which theoretically should separate the proteins under native, non-denaturing conditions.[35] In doing this, the authors showed that full length BACE1 (FL-BACE1) formed dimers while the BACE1 protein consisting of only the extracellular domain (NT-BACE1) clearly formed monomers.[35]

It was also demonstrated that altering the structure of the transmembrane domain of BACE1 did not interfere with its ability to form dimers, but once again reiterated that the presence of the domain is necessary for dimerization.[35] Finally, they showed that the FL-BACE1 had roughly 30-fold higher activity than that of the truncated version.[35]

Although the published evidence is compelling, there are a few areas of inconsistency and room for further study. For example, it is not clear whether BACE1 dimerization would withstand the heavy denaturing conditions of SDS-PAGE (visualized by Western blot), which usually remove secondary and tertiary structures. These results seem especially irregular because it was shown in the second study that no dimer was found for SDS-PAGE but only for BN-PAGE.[35] Secondly, it was reported that the dimerization was not influenced by either the type of transmembrane domain or membrane anchor present, but rather the mere presence or absence of a transmembrane domain. This contradicts with another report showing that a specific sulfur-rich, metal-ion binding motif (MxxxCxxxMxxxCxMxC) within the BACE1 transmembrane domain is required to initiate copper-mediated oligomerization.[33] These are just a few inconsistencies that need further investigation. One additional point is that co-localization experiments with BACE1 and APP, in tandem with protein extraction and imaging, alluded to the fact that that BACE1 dimerization may be dependent on specific interactions with substrate.[34,36]

1.5 Thesis Project Objectives

To address these outstanding questions and inconsistencies mentioned above and elucidate the nature of BACE1 dimerization in living cells, the goal of this thesis is to use non-invasive fluorescence micro-spectroscopic techniques to study BACE1 tagged with enhanced green fluorescent protein expressed in human embryonic kidney (HEK) cells. To date, no data has been published that has considered the dimerization event of BACE1 in its native environment within a living cell. In addition, we tested the hypothesis that dimerization is a function of substrate binding as put forth by the Multhaup group by carrying out our experiments to study the molecular events of BACE1 ranging from the millisecond to nanosecond timescale in the presence and absence of the BACE1 transition state analog peptide-statin inhibitor STA-200.

1.6 Thesis Chapters

The experimental design and setup for each technique used (i.e., confocal, differential interference contrast microscopy (DIC), fluorescence lifetime imaging microscopy (FLIM), fluorescence correlation spectroscopy (FCS) and fluorescence anisotropy) will be contained within its own chapter along with its contribution to the investigation of BACE1-EGFP expressed in HEK293 cells with and without STA-200 inhibition. Chapter 2 contains a comprehensive Materials and Methods section for the experiments performed, describing data acquisition as well as analysis with relevant figures and models. In Chapter 3, confocal and DIC are used to validate BACE1-EGFP

expression in HEK293 cells as well as to comment on overall cell health. Chapter 4 shows local and environmental factors that affect BACE1-EGFP by assessing the fusion protein's fluorescence lifetime. In Chapter 5, measurements from one-photon time-resolved fluorescence anisotropy (1P-trFA) is used to observe BACE1-EGFP rotation on the nanosecond timescale. Then, Chapter 6 presents studies on the translational movement and molecular brightness of BACE1-EGFP on the millisecond timescale. Each of these chapters stands alone with its own Abstract, Background, Results, Discussion, and Conclusions. Each technique will be presented with rationale, key measurements, figures, and data interpretation. Finally, Chapter 7 provides an overall conclusion of these studies with regards to dimerization of BACE1 in a cellular environment and offer insights on future directions.

Chapter 2

Materials and Methods

2.1 Materials

2.1.1 Human Embryonic Kidney Cell Culture (HEK293)

In these studies of BACE1, we used adherent human embryonic kidney cells (HEK293) as a model system. A flask of these cells was a generous gift from the laboratory of Dr. Lynne Bemis (Medical School, University of Minnesota Duluth;). Cells were grown in Eagle's minimum essential medium (EMEM) containing Earle's balanced salts [*Quality Biological, VWR International*]. To minimize autofluorescence background, the culture medium was prepared without phenol red, while containing 10% fetal bovine serum (FBS) + 2 mM L-glutamine + 50 U/mL penicillin/streptomycin. Cultured cells were incubated at 37 °C in a humidified 5% CO_2 atmosphere. For any given experiment, the HEK293 cells used had been passaged fewer than seventeen times.

2.1.2 BACE1-EGFP

The BACE1-EGFP construct was a generous gift from Dr. Bradley T. Hyman at the Harvard School of Medicine. The detailed protocol for constructing the BACE1-EGFP vector is described elsewhere.[29] Briefly, BACE1 was cloned from a Clontech whole human brain cDNA library using PCR and the following primers:

5′-AGCCACCAGCACCACCAGACTTG-3′ and 5′-ACTGGTTGGTAACCTCACCCATTA-3′.

The product was inserted into the pcDNA3.1/V5/His-Topovector (Invitrogen) (BACE1-V5). BACE1 was then cut out of BACE1-V5 at restriction sites HindIII and SacII and inserted into the pEGFP-N1 vector to create the BACE1-EGFP construct.

2.1.3 Fugene HD™ Transient Transfection

Fugene HD™ nonliposomal mediated transfection reagent was purchased from Promega (Madison, WI). HEK293 cells were grown to ~80% confluency at which point they were subcultured using 0.05% trypsin-EDTA solution without phenol red (Gibco). Cells were plated in MatTek 35 mm petri dishes (14 mm surface area, 0.16-0.19 mm thick microwell) at an approximate cell density of (2.1-3.2) x 10^4 cells/cm^2, 24 hours prior to being transiently transfected. The composition of the transfection solution was adjusted to give either a high- or low-efficiency transfection in order to tune the expression level of BACE1-EGFP as needed for each type of fluorescence measurement used in this project. The high-efficiency transfection solution consisted of 245 µL of culture media without antibiotics, 5.0 µg of BACE1-EGFP DNA with 15 µL of Fugene HD™ per 35 mm plate while the low-efficiency transfection solution consisted of 49.7 µL of culture media without antibiotics, 0.1 µg of BACE1-EGFP DNA with 3.75 µL of Fugene HD™ per 35mm plate. Cells were incubated in transfection media for 24-48 hours, and then the transfection solution was replaced with complete culture media with

antibiotics (without phenol red) at least 1 hour before conducting microscopy or spectroscopy measurements.

2.1.4 Inhibition

We used STA-200, a statine-containing BACE1 transition state analog (Lys-Thr-Glu-Glu-Ile-Ser-Glu-Val-Asn-(Statine)-Val-Ala-Glu-Phe-OH) to inhibit BACE1 cleavage of endogenous substrate. The corresponding biophysical studies under STA-200 inhibited conditions allow us to examine the role of substrate binding on the dimerization hypothesis of BACE1-EGFP being tested in this project. All reported biophysical measurements on BACE1-EGFP in this thesis were carried out under both untreated and STA-200 inhibited conditions. Inhibition of BACE1 was achieved using 2 mL of culture media with 1 µL of the stock STA-200 solution (100 µM in 2% DMSO) to give a final concentration of 50 nM.[22] Cells were incubated with the inhibitor for at least 1 hour prior to measurements. Our rationale in these inhibition-based studies was not only to examine the effect of substrate/inhibitor binding on dimerization, but also to prevent BACE1-EGFP binding to endogeneous substrates.

2.2. Methods and Data Analysis

2.2.1 Confocal and DIC Microscopy

Conventional laser scanning confocal microscopy, equipped with differential interference contrast (DIC) for assessing cell morphology, were used to image the localization and distribution of BACE1-EGFP in cultured HEK cells at room temperature. The confocal and DIC imaging system has been described in detail

elsewhere.[37] Briefly, the confocal microscope consists of an inverted microscope (Olympus, IX81), equipped with a 1.2-NA, 60X water immersion microscope objective. The inverted microscope was coupled with a laser-scanning unit (FV300, Olympus) that was fiber coupled with multiple laser lines (Ar-Ion Laser: 488 nm; Compact solid-state Lasers: 561, 641 nm), which was controlled by a Cobalt Jive 50 unit (Olympus). Based on the absorption (maximum at 488 nm) and emission (maximum at 510 nm) spectra of EGFP, cells expressing BACE1-EGFP were excited using 488 nm (Ar-ion laser). Fluorescence was viewed first using Hg lamp and FITC filter cube prior to being imaged using 510IF Filter. The confocal system is diagrammed in Figure 2.1 and additional information about confocal microscopy can be found elsewhere.[38] Data acquisition and analysis were carried out using the Fluoview 300 software (Olympus) for 3-D and time-series imaging. This laser scanning confocal microscope was modified to allow for two-photon (2P) fluorescence, FLIM, and 1P-trFA imaging (see below).

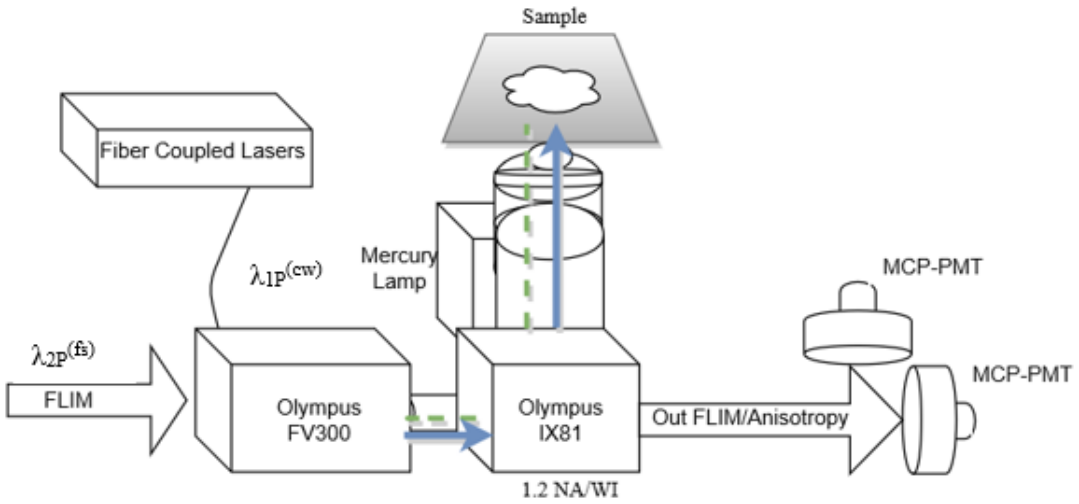

Figure 2.1: A Diagram Describing Our Confocal and DIC Microscopy System

2.2.2 *Two-Photon Fluorescence Lifetime Imaging Microscopy (FLIM)*

The 2P fluorescence microscopy and fluorescence lifetime imaging microscopy (FLIM) system was described in detail elsewhere.[37] Briefly, femtosecond laser pulses (120 fs, 76 MHz) used in 2P microscopy were generated using a Titanium-Sapphire solid state laser system (Mira 900-F, Coherent), pumped by a diode laser (10 W, Verdi-10W, Coherent). The fundamental excitation wavelength ranged from 700 to 1000 nm and was extended from 350 to 500 nm using a second harmonic generator (SHG 4500, Coherent). In these measurements on BACE1-EGFP, however, we used 930 nm and 465 nm for two-photon FLIM and 1P-trFA, respectively, as described below. For 2P fluorescence imaging and FLIM, the 930 nm pulses were steered toward the modified FV300 laser-scanning unit described above to excite the cultured cells expressing BACE1-EGFP using a 1.2 NA, 60X, water-immersion objective.

For FLIM measurements, the 2P-epifluorescence was isolated from the excitation laser using a dichroic mirror (DM690LP) and filters (475 Russian Blue and 690SP filters) before being detected at magic angle (Glan-Thompson Polarizer set at 54.7°) using a microchannel plate photomultiplier tube, MCP-PMT (R3809U, Hamamatsu). The fluorescence signal was then amplified (GMbH amplifier model, Becker & Hickl), routed (HRTxx, Becker & Hickl), and recorded using SPC-830 module (Becker and Hickl). The SPC-830 module was synchronized (in the reverse mode) with a fast photodiode signal, SYNC, (400N, Becker & Hickl), which was triggered by a small fraction of the excitation laser using a coverslip (~2%). The delay time between the SYNC pulse and the molecular excitation pulse was controlled using a 7 ft coaxial cable. The operation of the SPC-830

module is based on principles of the time-correlated single-photon counting (TCSPC) technique.[39] To obtain a good signal-to-noise ratio, the TCSPC histogram for each FLIM image was recorded over 3-5 minutes, which varied based on the expression level of BACE1-EGFP in the cultured HEK cells. For each FLIM image, the corresponding confocal and DIC images were recorded to ensure negligible two-photon laser-induced photobleaching of the labeled protein or photodamage to the cells. Over the course of these measurements, a magnification range of 3-5 was used. Figure 2.2 provides a sketch that describes our FLIM system. The average infrared laser power at the sample (maximum 10 μW) was controlled using a neutral density filter to ensure negligible BACE1-EGFP photobleaching and photodamage to the cells.

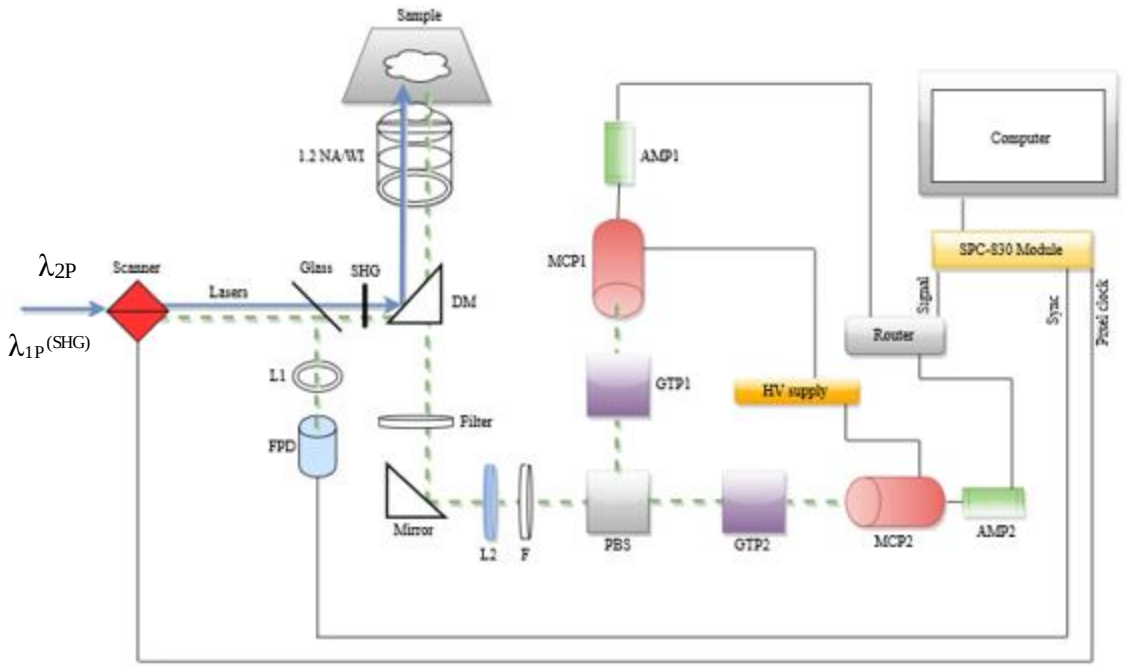

Figure 2.2: A Diagram of Our Two-photon FLIM System. Laser: 930 or 465 nm pulses; L: lens; FPD: fast photodiode for SYNC signal; DM: dichroic mirror, F: filters; PBS: polarizing beam splitter, GTP: Glan-Thompson Polarizer; MCP: microchannel plate PMT, AMP: amplifier; HV Supply: high voltage (-2.9 kV) power supply.

The acquired FLIM images were analyzed using the SPCImage software (Becker & Hickl), which uses a non-linear least-square fitting routine (Levenberg-Marquardt algorithm) for each fluorescence decay per pixel. The majority of 2P fluorescence decays in each FLIM image were described satisfactorily using a single exponential decay model (Eq 2.1) such that:

$$F(t) = \left(F_0 * e^{-\frac{t}{\tau_{fl}}} \right) \otimes IRF \qquad \text{(Eq. 2.1)}$$

where F_0 is the initial fluorescence intensity and τ_{fl} is the fluorescence lifetime of BACE1-EGFP. Each decay per pixel was deconvoluted with a computer-generated instrument response function (IRF) with a full-width half-maximum (FWHM) that depends on the measured rise of the fluoresce decay.[39] The quality of the fit was judged using both $\chi^2$and the residual.[39] In our 2P FLIM measurements on HEK cells expressing BACE1-EGFP, images with 256 x 256 pixels were constructed with 64 time bin per pixel (i.e., 259 ps/bin). In addition, the upper signal level (binning = 2) in each FLIM image used in these analyses was at least 9000 photon counts per pixel (maximum) and showed good signal-to-noise fluorescence decays. The system was calibrated using a solution droplet of Rhodamine Green (RhG, 2.0 μM) which yielded a single exponential decay with an average fluorescence lifetime of 3.9 ns in agreement with literature values.[40] Similar measurements were carried out on free EGFP in a buffer (PBS, pH 7.4, 10 μM) which yielded a single exponential decay with an average fluorescence lifetime of 2.5 ns. A screen shot of SPCImage for a typical 2P-FLIM image of HEK cells expressing BACE1-EGFP under untreated conditions (Figure 2.3) shows an example of FLIM data and data analysis used in this project.

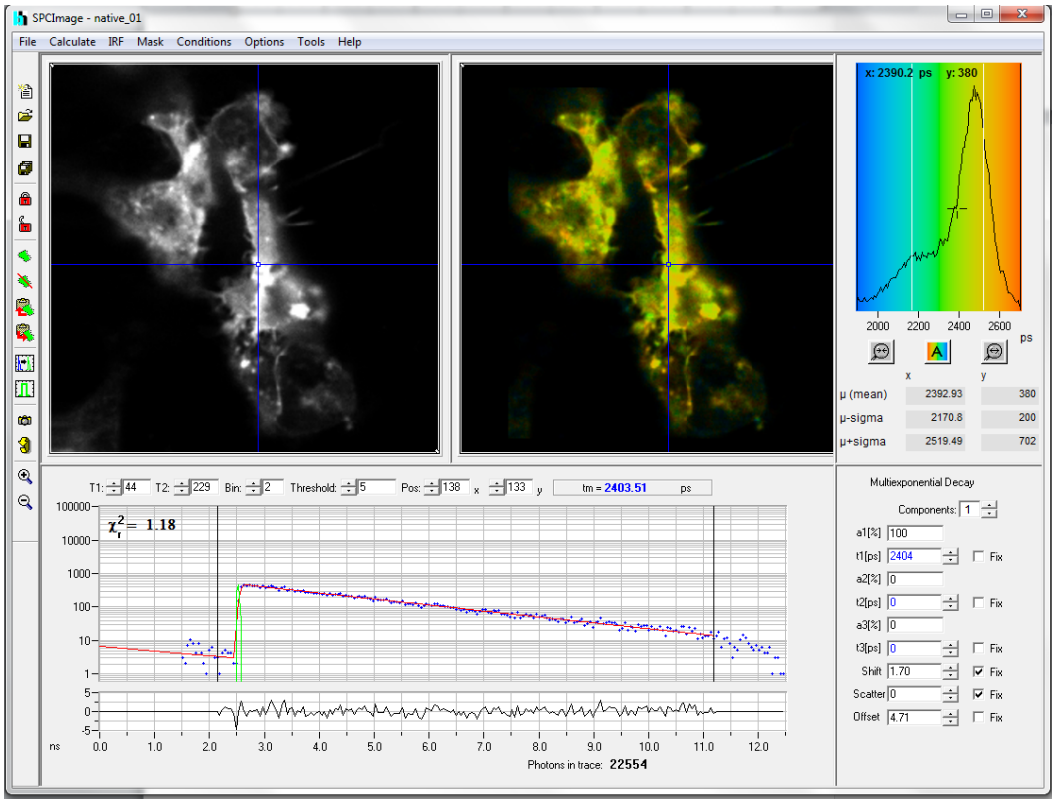

Figure 2.3: A Screenshot of SPCImage Data Analysis.

The left image shows the 2P-fluorescence intensity with the corresponding 2P-FLIM matrix on the right. Each pixel in the FLIM image can be fitted with models containing up to three exponential decays and the corresponding fitting parameters are shown at the right of the screen shot (a_1, τ_1, etc…). For any pixel in the FLIM image, the corresponding fluorescence decay (along with the fitting curve as well as χ^2 and residual) can be seen (center). The fluorescence lifetime distribution for each FLIM image is shown in the upper right corner.

In these FLIM image analyses, we have carefully chosen binning parameters that maximize the signal-to-noise ratio for the fluorescence decay without significant loss of

spatial resolution due to averaging neighboring pixels (i.e., binning). We noticed, for example, that as we increased the binning from 1 to 10, the signal-to-noise ratio of the observed fluorescence decays increased tremendously, but the pixel-resolution (i.e., spatial information) was poor (averaged out). We also observed that the FLIM image lifetime-frequency histogram (Figure 2.4) became narrower (smaller FWHM around the mean average lifetime, 2.5 ns in this case) with an increased frequency of the pixels corresponding to the average fluorescence lifetime. However, spatial information was lost for the BACE1-EGFP population with a shorter lifetime (left shoulder of the histogram, Figure 2.4). Based on these findings, we decided to use binning of 2-3 throughout this project. A binning of 1 groups the central and immediately adjacent pixels to calculate the average intensity/decay. A binning of 2, however, would include the central pixel plus 2 rows of surrounding pixels for average calculations. This allowed us to strike a nice balance between the spatial information and signal-to-noise ratio for reliable FLIM measurements of BACE1-EGFP in cultured HEK cells under different physiological conditions. Some balancing is required because although the χ^2 value for goodness-of-fit also increases as binning increases, there is a corresponding decrease in the information content (spatial resolution) of the data resulting in less appropriate model fitting. This deviation of fitting quality (observed by χ^2) is not surprising when averaging over large, heterogeneous locations in living cells with an excellent signal-to-noise ratio for each decay.

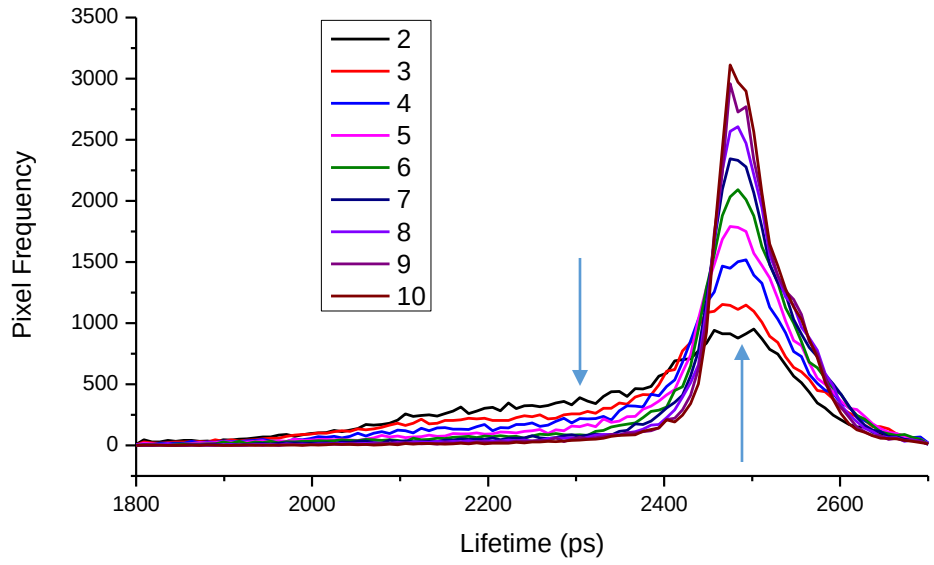

Figure 2.4: Effects of Binning on Fluorescence Lifetime as a Function of Pixel Frequency. As the colors of the colors of the graph go from black to brown, the binning of the decay matrix increases from 2 to 10. By doing this the shoulder lifetimes, from 2.1 ns to 2.4 ns, decrease while the peak lifetimes around 2.5 ns increase. Optimization of this parameter is essential to obtain adequate signal-to-noise levels while maintaining spatial resolution.

The SPCImage software also allows for analyzing FLIM images weighted as a function of pixel frequency and pixel intensity. For the representative FLIM image shown in Figure 2.5, both weighting options yield the same mean fluorescence lifetime per FLIM image (2.5 ns in this case), where the signal-to-noise ratio was very good by FLIM standards. However, the weighted frequency mode of analysis provided valuable information concerning a population of BACE1-EGFP with a shorter lifetime (2.3 ± 0.1 ns), which was washed out in the intensity-weighted mode of analysis (Figure 2.5).

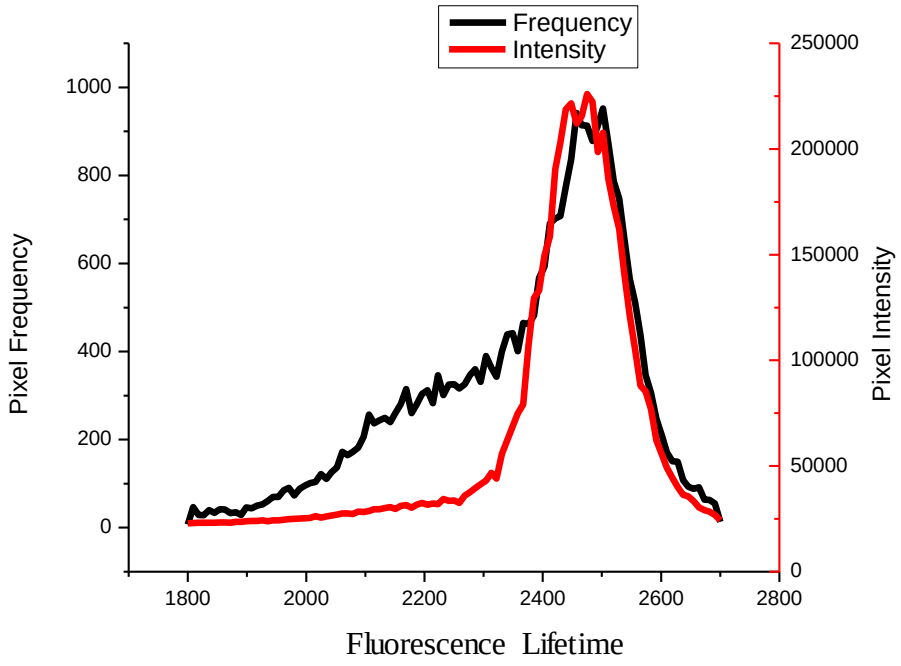

Figure 2.5: Representative Histograms for Different FLIM Analysis Modes using SPCImage. Fluorescence lifetime histogram as a function of pixel frequency (black) or pixel intensity (red).

Based on these findings, we decided to use frequency-weighted analysis of FLIM images throughout this thesis. This is especially valid in light of the high signal-to-noise ratio in our FLIM measurements of HEK cells expressing BACE1-EGFP.

2.2.3 Time-Resolved Fluorescence Anisotropy Using TCSPC Technique

The tumbling motion (or rotational time) of BACE1-EGFP in cultured cells was characterized using 1P time-resolved anisotropy measurements as a means to assess both the structural flexibility of the construct and homo-FRET (fluorescence resonance energy transfer between like molecules). Time-resolved anisotropy measurements can be carried out using the TCSPC technique as was the case with 2P-FLIM (see above) with minor modifications of the excitation and detection configurations as described elsewhere in great detail.[41]

The rotational time of BACE1-EGFP (~75 kDa) in the restricted cell environment is expected to be much slower than the excited-state fluorescence lifetime of EGFP free in solution (~2.8 ns). [42] As a result, the repetition rate of the excitation pulses was reduced from 76 MHz to 4.2 MHz, with 286 ns between pulses. This enabled the monitoring of the rotational motion of large, restricted proteins that might not be complete within 13 ns. The repetition rate of 4.2 MHz of the femtosecond laser pulses (see above) was achieved using a pulse picker (Coherent, *Mira 9200*). The 4.2 MHz infrared (IR) laser pulses (horizontally polarized) were steered and conditioned prior to generating the second harmonic laser pulses at 465 nm using second harmonic generation (SHG 4500, Coherent), which were then used for 1P-trFA measurements. The vertically

polarized 1P laser pulses were steered to the back exit of the IX81 microscope, which also allowed for the Hg lamp spectral lines for visual inspection of the cultured cells expressing BACE1-EGFP. In addition to the dichroic mirror (467 – 556 nm), excitation (475/50) and detection (531/40 and Russian Blue) filters were carefully chosen to selectively detect the fluorescence emission without scattered laser light. The depolarized fluorescence of BACE1-EGFP in cultured HEK cells was resolved into parallel and perpendicular polarizations using a polarizing beam splitter (CM1-PBS251, ThorLabs) and detected simultaneously using two MCP-PMTs as described above for FLIM. The polarization-analyzed fluorescence photons were then amplified, routed, and registered in SPC-830 module. The resulting time-resolved fluorescence decays (histograms) were then recorded for both parallel and perpendicular (with respect to the excitation laser polarization) fluorescence using SPCImage. For time-resolved anisotropy, the G-factor (Geometrical factor) accounts for potential polarization-biased detection and can be estimated using the tail-matching approach of a small molecule such as Rhodamine Green (rotational time of 130 ps compared to a 3.9 ns fluorescence lifetime).[43] In our setup, the geometrical (G) factor is ~0.6 under the experimental conditions reported here. Anisotropy decay analyses were carried out using OriginPro (8.1) software.

The measured parallel and perpendicular fluorescence decays are then used to calculate the corresponding anisotropy using the following equation (2.2):

$$r(t) = \frac{F_{II}(x,y,z) - G * F_{\perp}(x,y,z)}{F_{II}(x,y,z) + 2 * G * F_{\perp}(x,y,z)} \qquad (2.2)$$

where *r*, *F*, and *G* are defined as the anisotropy, fluorescence intensity, and *G*-factor, respectively. Based on the molecular and cellular complexity as well as the potential presence of more than one species, the time-resolved anisotropy decays can generally be described as a multiexponential decay (Eq. 2.3) such that:

$$r(t) = \beta_1 * e^{-t/\phi_1} + \beta_2 * e^{-t/\phi_2} \quad \text{(Eq. 2.3)}$$

where β, *t*, and ϕ are the anisotropy amplitude (initial anisotropy = $r_0 = \beta_1 + \beta_2$), time, and rotational time, respectively. In the course of our measurements of the rotational motion of BACE1-EGFP in cultured HEK cells, the anisotropy decays were described satisfactorily with two exponential decays (Eq. 2.3). It is worth noting that the measured rotational time (ϕ) depends on both the volume (*V*) of the tumbling moiety and the viscosity (η) of the surrounding environment such that (Eq. 2.4):

$$\phi = \eta V / k_B T \quad \text{(Eq. 2.4)}$$

where η, *V*, *T*, and k_B are the viscosity, hydrodynamic volume of the tumbling species, temperature, and the Boltzmann constant, respectively. In the Stokes-Einstein model, the rotational diffusion coefficient (D_R) equals $1/6\phi$ for spherical molecules.

2.2.4 Fluorescence Correlation Spectroscopy (FCS)

To examine whether BACE1-EGFP forms a dimer, we used fluorescence correlation spectroscopy (FCS) to characterize its translational diffusion coefficient, which is inversely proportional to the hydrodynamic radius of the diffusing species. The experimental setup, FCS modalities, and data analysis were described in great detail

elsewhere.[41] Briefly, an inverted microscope (XI81, Olympus) was fiber coupled to multiple continuous wave lasers with wavelengths of 488 nm (Coherent Sapphire 488-20), 561 nm (Cobolt Jive^{TM}), and 641 nm (Coherent Cube). The microscope was also equipped with wide-field and total internal reflection (TIRF) imaging capabilities using an EM-CCD camera (Evolve, Photometrics). The microscope, imaging data acquisition, and laser-wavelength selection were controlled using the Metamorph software. A home-built FCS setup coupled with the inverted microscope at the right exit-port allowed for autocorrelation and cross-correlation spectroscopy (Figure 2.6). For HEK cells expressing BACE1-EGFP, 488 nm excitation was used via FITC filter cube (excitation and detection filters 467-498 nm, 513-556 nm, respectively, and a 467-556 nm dichroic mirror) and the corresponding epi-fluorescence was steered toward the right exit-port, filtered (400-700 nm), and tightly focused on an optical fiber (50 nm in diameter) that acts as a confocal pinhole. The fluorescence signal was then detected using one (for autocorrelation analyses as in these studies) or two (for cross-correlation analyses) avalanche photodiodes (APDs, SPCM CD-2969, Perkin-Elmer, Fremont, California). The signal was then amplified, detected, and correlated using external multiple-tau-digital correlator (ALV/6010-160, Langen/Hessen, Germany), with the ALV-Correlator software used for FCS data acquisition. The FCS experimental setup is shown in Figure 2.6.

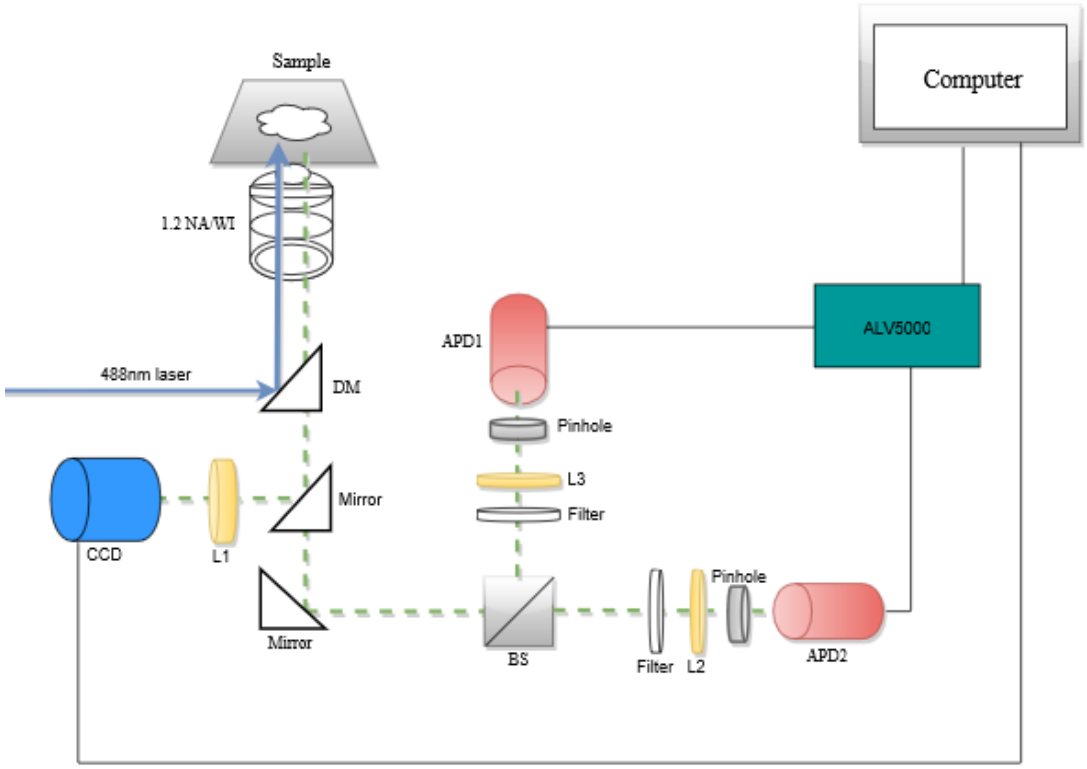

Figure 2.6: Diagram of Our Multimodal Fluorescence Correlation Spectroscopy System that Allows for Autocorrelation and Cross-correlation CCD: Charge Coupled Device Camera, DM: Dichroic Mirror, NA: Numerical Aperture, L: Focusing Lense, BS: Beam Splitter, APD: Avalanche Photodiode, ALV5000: multiple-tau-digital correlator. The FCS system was coupled with multiple solid-state lasers (488, 561, and 641 nm) via optical fibers.

The FCS setup was calibrated and optimized on a daily basis using Rhodamine Green (60 nM, PBS, pH 7.4) with a known diffusion coefficient of 2.8 x 10^{-6} cm^2/s.[37] Rhodamine Green is a photostable fluorophore with a fluorescence quantum yield of 0.95 and a steady-state spectroscopy (both absorption and emission spectra) that is fairly similar to our BACE1 label (i.e., EGFP).[37,44,45] Under the same calibration conditions, fluorescence fluctuation autocorrelation measurements were taken for BACE1-EGFP in the plasma

membrane of HEK cells; the laser was randomly focused throughout the cell membrane under both untreated and inhibited conditions. The measurements were repeated on different cells, dishes, and days to ensure reproducibility and avoid any systematic errors. Fluorescence (or concentration) fluctuation of a single molecule diffusing through an open observation volume can be caused by translational diffusion and chemical reactions as shown in Eq. 2.5:[46]

$$\frac{\partial}{\partial t}\delta C_i(r,t) = D_i\nabla^2\delta C_i(r,t) + \sum_j T_{ij}\ \delta C_i(r,t) \qquad \text{(Eq. 2.5)}$$

where C_i is the concentration, D_i is the diffusion coefficient of the i^{th} species, and T is temperature in Kelvin. The first term of Eq. 2.5 represents the time-dependence of the concentration fluctuation due to diffusion, while the second term accounts for that due to any chemical reactions that may be present. The corresponding fluorescence fluctuation autocorrelation of a diffusing species provides invaluable information about the translational diffusion coefficient and underlying chemical and photo-physical processes of the molecule under investigation. Fluctuations in the concentration will cause a fluctuation in the fluorescence signal, and the corresponding fluorescence fluctuation autocorrelation function, $G(\tau)$, can be calculated using Eq. 2.6.[44]

$$\mathrm{G}(\tau) = \frac{\langle \delta F(t) * \delta F(t+\tau) \rangle}{\langle F \rangle^2} \qquad \text{(Eq. 2.6)}$$

where $\delta F(t)$ is the fluorescence fluctuation at time t and τ is the correlation lag time. For a Gaussian (lateral) and Lorentzian (axial) observation volume, the 3D autocorrelation function depends on both the average number of molecules (N) residing in the observation volume and the diffusion time (τ_D) such that [46]:

$$G(\tau) = \frac{1}{N} * \left\{ \left[\frac{1}{1+\left(\frac{t}{\tau_D}\right)} \right] + \left[\frac{1}{1+\left(\frac{t}{\tau_D * \omega_0{}^2}\right)} \right]^{0.5} + C \right\} \qquad \text{(Eq. 2.7)}$$

where N is the average number of molecules at any given time, τ_D is the residence time of a molecule in the observation volume, and ω_0 is the structure parameter that describes the observation volume. The structure parameter is simply the ratio of the axial (z_0) to the lateral (ω_{xy}) extension of the observation volume.

A typical fluorescence autocorrelation of Rhodamine Green (PBS, pH 7.4) is shown in Figure 2.7 with an estimated diffusion time of 0.12 ms at room temperature.

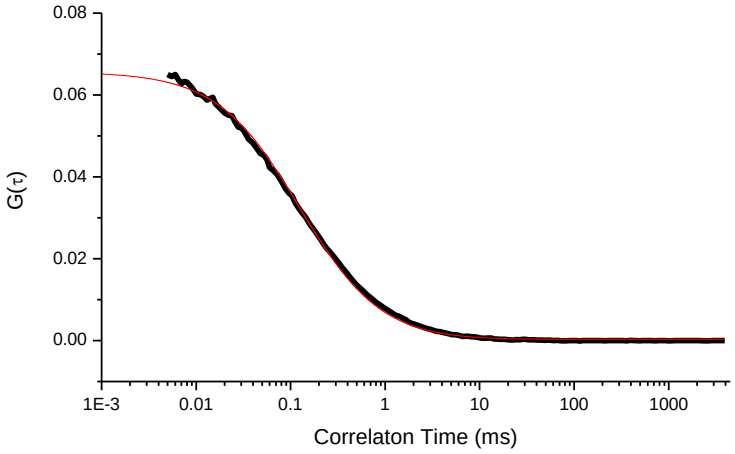

Figure 2.7: Autocorrelation Curve of Rhodamine Green at Room Temperature.

However, for BACE1-EGFP in the plasma membrane of living HEK cells, we found that the corresponding autocorrelation function *(G(τ))* can be modeled as two-diffusing species in a 2D membrane such that: [47]

$$G(\tau) = \frac{1}{N} * \left\{ (1-f) * \left[\frac{1}{1+\left(\frac{t}{\tau_1}\right)} \right] + f * \left[\frac{1}{1+\left(\frac{t}{\tau_2}\right)} \right] \right\} \qquad \text{(Eq. 2.8)}$$

where N is the number of molecules, f is the population fraction of a species 2 with a diffusion time τ_2. The corresponding population fraction of species 1 with a diffusion time τ_1 is (1-f). The corresponding translational diffusion coefficient (D_T) relates to both the measured diffusion time (τ_1 or τ_2, also known as τ_D) and the lateral radius (ω_{xy}) of the open observation volume such that: [41]

$$\tau_D = \frac{\omega_{xy}^2}{4D_T} \qquad \text{(Eq. 2.9)}$$

In the Stokes-Einstein model, the translational diffusion coefficient (D_T, cm^2/sec) of a spherical molecule depends on temperature (T), viscosity (η), and the hydrodynamic radius (a) such that [46]:

$$D_R = \frac{k_B T}{6\pi\boldsymbol{\eta a}} \qquad \text{(Eq. 2.10)}$$

where k_B is the Boltzmann constant, T is the temperature in Kelvin, η is the viscosity (g/cm·sec), and a is the hydrodynamic radius of a single diffusing species under investigation. The measured diffusion time using FCS will then be used to calculate the diffusion coefficient, which can then be used to examine the size of the diffusing species (i.e., monomeric or dimeric BACE1-EGFP).

In the Saffman-Delbrück model, the translational diffusion coefficient of a transmembrane protein (modeled as a cylindrical molecule through a membrane) depends on temperature, the viscosity of both the membrane (η_m) and surrounding media (e.g., culture media and the cytosol; η_w), hydrodynamic radius (a), and membrane thickness (h) such that: [41]

$$D = \frac{k_{B*}T}{(4\pi\eta_m h)}\left[\ln\left(\frac{\eta_m h}{\eta_w a}\right) - 0.5772\right] \qquad \text{(Eq. 2.11)}$$

The calibrated observation volume using RhG in a buffer (3D) was used to calculate the lateral extension of the observation volume associated with BACE1-EGFP in the plasma membrane (2D) such that:

$$\frac{\tau_i}{\tau_{RhG}} = \frac{D_{RhG}}{D_i} \qquad \text{(Eq. 2.12)}$$

where τ and D are the diffusion time and diffusion coefficient for RhG and the i^{th} species, respectively.

Chapter 3

Visualization of BACE1-EGFP Expression in HEK293 Cells

3.1 Summary

To study BACE1 in living cells, we obtained BACE1 genetically engineered with EGFP and transiently transfected HEK293 cells with the BACE1-EGFP plasmid. The expression level of BACE1-EGFP in cultured HEK cells was optimized by varying construct and transfection reagent concentrations. The distribution of BACE1-EGFP within the cell was visualized using both laser scanning confocal and differential interference contrast (DIC) microscopies. Our results indicate that the fusion protein is localized at the plasma membrane and in the Golgi apparatus. Similar measurements were made following inhibition of BACE1 using the STA-200 inhibitor. The compartmentalization of BACE1-EGFP in cells incubated for 24 hours following transfection is consistent with our current understanding of BACE1 cell biology. In addition, we observed no adverse side effects on cell viability (e.g., apoptosis) with different levels of BACE1-EGFP expression or inhibition with STA-200. These studies are essential for establishing baseline controls for our biological system as a reference point for the spectroscopy measurements described in the following chapters.

3.2 Background

The first step in elucidating the oligomeric state of BACE1 using fluorescence-based methods that are both quantitative and non-invasive entails fluorescence labeling of the target protein (BACE1 in this case) in cultured, living cells. Our fluorescence label of choice was genetically encoded EGFP, which exhibits large fluorescence quantum yield with negligible photobleaching.[48] The BACE1-EGFP fusion protein consists of the full-length BACE1 transmembrane aspartyl protease (~75 kDa) along with an enhanced green fluorescent protein (EGFP, ~27 kDa) attached at the C-terminus by a 12 amino acid linker.[29] The Hyman group demonstrated that BACE1-EGFP fusion protein was successfully engineered and expressed within N2a cells.[29] von Arnim *et al.* demonstrated that BACE1-EGFP exhibited the expected BACE1 trafficking pattern and was expressed in the ER, TGN, membrane, and early endosomes.[29] To validate the construct, Hyman and coworkers introduced a BACE1-APP shedding assay to demonstrate β-secretase activity of the expressed BACE1-EGFP fusion protein.[29]

We expressed the BACE1-EGFP fusion protein in human embryonic kidney cells (HEK293) as our model system. The BACE1-EGFP plasmid was a generous gift from Dr. Bradley T. Hyman at the Harvard School of Medicine. The HEK293 cell line was chosen due to the fact that it has been extensively used as a model system in the study of secretase enzymes.[27,29,34,35] This cell line also exhibits certain similarities with human neurons such as expression of neuronal voltage-gated to potassium, sodium, and calcium channels .[49] In addition, HEK293 cells have been known to respond to neuronal stimuli such as neurotensin and acetylcholine.[49] Previous studies involving BACE1 have

employed the HEK293 cell line as a model system as a starting point prior to moving on to other potentially more relevant, neural cell lines.[29,50] Additional advantages of the HEK cell line include ease of transfection with BACE1-EGFP vector and the fact that it is a robust, adherent cell line that is easily cultured. Also, HEK293 cells express minimal amounts of endogenous APP which may reduce the effects of STA-200 inhibition.

3.3 Materials and Methods

As described in Chapter 2, we followed the work of Hyman and co-workers to express BACE1-EGFP in cultured HEK293 cells using non-liposomal mediated transient transfection.[29] As mentioned, the BACE1-EGFP plasmid was a generous gift from Dr. Bradley T. Hyman. Prior to our spectroscopy measurements, we used confocal and DIC imaging to assess cell viability as well as BACE1-EGFP expression level and distribution within the cell. See Chapter 2 (Materials and Methods) for additional information concerning BACE1-EGFP transfection and inhibition as well as HEK cell culture.

3.4 Results and Discussion

3.4.1 Three-Dimensional Visualization of BACE1-EGFP Expression in Adherent HEK Cells

Typical confocal and DIC images of HEK cells expressing BACE1-EGFP are shown in Figure 3.1. These images were recorded under untreated conditions following transient transfection with BACE1-EGFP plasmid. These images were recorded using 488 nm illumination of different cross-sections throughout the cell including the middle of the cell (Figure 3.1 A) and near the glass substrate (Figure 3.1 B). These confocal and DIC images show that cultured HEK cells express BACE1-EGFP at levels suited for two-photon FLIM and time-resolved anisotropy (see Chapter 4 and 5). However, this expression level will be too high for single-molecule fluctuation analysis using FCS (Chapter 6).

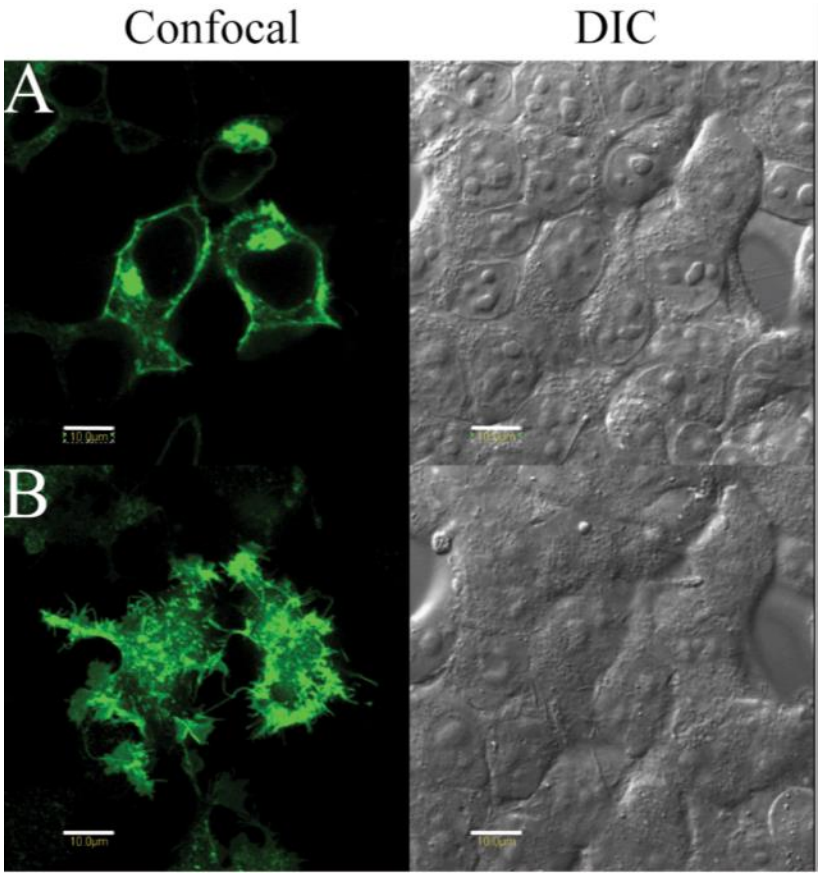

Figure 3.1: Confocal and DIC Analysis of Untreated HEK293 Expressing BACE1-EGFP.
Panel A: cross-section, Panel B: HEK293 cell-glass surface interface. Confocal (left), DIC (right).

We were able to manipulate the cell expression level of BACE1-EGFP using a lowered concentration of vector during the transfection process for FCS studies. In addition, the cross-sectional confocal and DIC images of the cultured cells (Figure 3.2) reveal that the BACE1-EGFP fusion protein is expressed in the plasma membrane (dotted arrow, PM) as well as in the Golgi apparatus (solid arrow); this is consistent with expected trafficking of BACE1.[2] These confocal and DIC images also show that BACE1-

EGFP is excluded from the nucleus (Figure 3.2). Collectively, these results demonstrate that neither the transfection process nor the transient expression of BACE1-EGFP had any apparent adverse effects on the overall cell viability

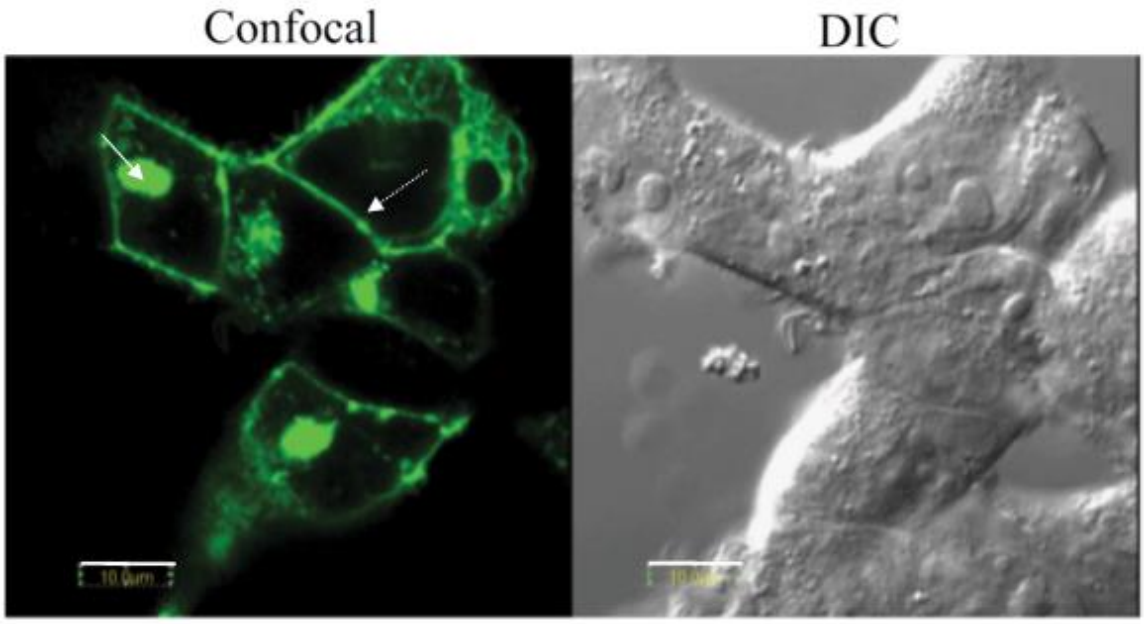

Figure 3.2: Expression of BACE1-EGFP Localized to Plasma Membrane and Golgi Apparatus. Confocal (left), DIC (right), arrows in confocal highlighting Golgi apparatus (solid arrow) and plasma membrane (dotted arrow).

3.4.2 Monitoring STA-200 Inhibition of BACE1-EGFP Expression in Adherent HEK Cells

Next, we examined the effects of BACE1 inhibition on expression and overall cell health using the transition state analog STA-200. To do this we incubated HEK293 cells with 50 nM STA-200 (concentration was selected based on IC_{50} values of ~30 nM from purified BACE1 assays [19]) for at least one hour prior to imaging using confocal and DIC

microscopy. The rationale for use of STA-200 is based on evidence suggesting that BACE1 dimerization is a function of substrate binding (e.g., APP in this reference).[34] Although endogenous expression of APP in human kidney cells is minimal, [51] STA-200 will block the BACE1-EGFP active site and should prevent any other potential substrates from inducing BACE1 dimerization as seen by Sinha *et al.*[19]

Typical images of HEK293 cells expressing BACE1-EGFP in the presence of STA-200 (50 nM) are shown in Figure 3.3. As with the confocal and DIC images of the untreated cells, those in the presence of inhibitor show adequate expression of fusion protein as well as signs of healthy morphology as previously described. This suggests the STA-200 inhibitor exhibits no significant effects on overall cell health and BACE1-EGFP expression. Therefore, measurements taken with various micro-spectroscopic methods will not be skewed by inhibition-induced factors such as apoptosis or reduced expression.

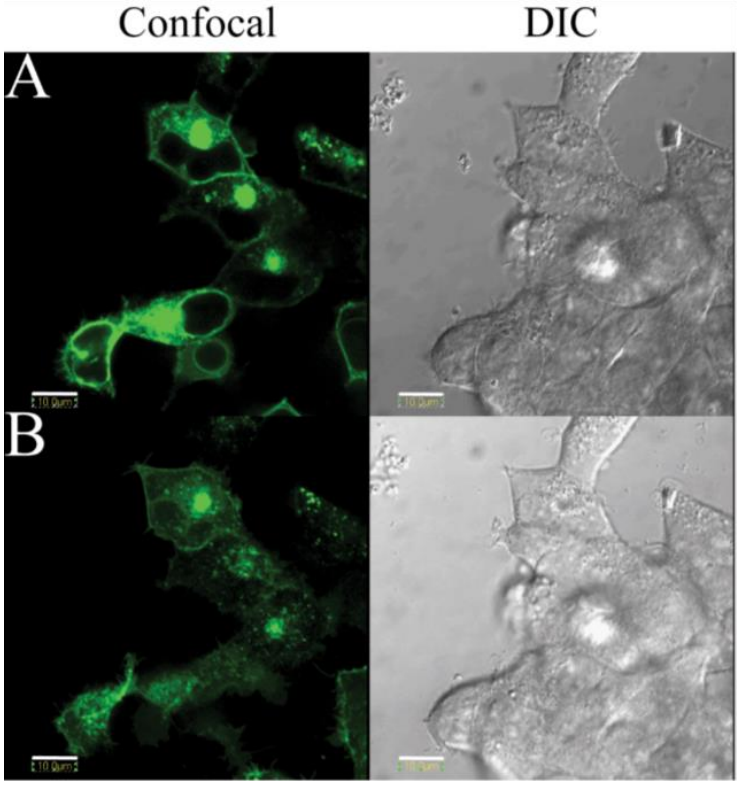

Figure 3.3: Confocal and DIC Analysis of STA-200 Inhibited HEK293-BACE1-EGFP. Panel A: cross-section, Panel B: HEK293 cell surface-glass coverslip interface. Confocal (left), DIC (right).

3.5 Conclusions

To study BACE1 in a cellular environment, we utilized a genetically engineered fusion protein composed of BACE1 linked to EGFP. We employed the use of confocal and DIC microscopy to study protein expression as well overall cell health both in an untreated environment as well as in the presence of STA-200 inhibitor. Based on results from our confocal microscopy, we were successful in transiently transfecting HEK293 cells to produce BACE1-EGFP fusion protein that localized to the plasma membrane as well as the Golgi apparatus; this is consistent with what is expected for BACE1. Both the

BACE1-EGFP transfection and STA-200 inhibition processes had no apparent negative effects on the morphology or overall health of the cells as conformed by DIC. This leads us to believe that in the following chapters, measurements will not be influenced by factors such as apoptosis or reduced BACE1-EGFP expression. With confirmation of correct expression and localization of BACE1-EGFP, measurements using different micro-spectroscopic techniques can be used to observe BACE1-EGFP as a monomer or dimer in its respective cellular locations. With this in mind, the next question we wanted to ask was: how is BACE1-EGFP influenced by local effects of such conformational and environmental changes? To answer this question, we turned to the time-correlated single-photon counting technique FLIM.

Chapter 4

Examining the Sensitivity of BACE1-EGFP to Conformational and Environmental Changes in HEK293 Cells

4.1 Summary

BACE1 is hypothesized to dimerize in living cells, which, may influence Aβ production. To test this dimerization hypothesis, we used two-photon fluorescence lifetime imaging microscopy (FLIM) on transiently transfected HEK cells expressing BACE1-EGFP. Excited-state fluorescence lifetime is known to be sensitive to changes in both the chemical structure of a given fluorophore (e.g., dimerization of BACE1-EGFP) and its surrounding local environment. These measurements were carried out using 930 nm excitation of cultured HEK cells under untreated and STA-200 inhibited conditions. As a control, the corresponding confocal and DIC images were recorded after each 2P-FLIM to ensure negligible photodamage or photostress to the cells. The observed fluorescence decay per pixel for cellular BACE1-EGFP is described satisfactorily using a single-exponential decay model under FLIM conditions, which is consistent with the protective nature of the β-barrel of EGFP. However, the frequency-weighted histogram of each FLIM image indicates two populations of BACE1-EGFP throughout the cell that fit double Gaussian distributions. These distributions along with the 2P-FLIM images revealed two sub-populations of BACE1-EGFP each with a distinct mean fluorescence lifetime value. The dominant population centered on 2.45 ± 0.18 ns is attributed to monomeric BACE1-EGFP in living cells with a refractive index greater than that of EGFP in buffer. A minor population exhibiting a mean lifetime of 2.2 ± 0.3 ns was attributed to homo-FRET of dimeric BACE1-EGFP. The addition of the BACE1

inhibitor STA-200 had noticeable though not statistically significant effects on the magnitude of the relative lifetime distributions at the cell membrane. Under STA-200 inhibited conditions, for example, the FWHM of the shorter lifetime population histogram increased, while the FWHM distribution for the longer lifetime population decreased. This observation suggests that the dimerization of BACE1-EGFP in HEK293 cells may be dependent on substrate binding.

4.2 Background

Two-photon (2P) fluorescence lifetime imaging microscopy (FLIM) is the tool of choice for examining conformational and environmental changes of fluorescently tagged proteins in cells with great sensitivity.[52] One-photon (1P) FLIM has been used previously to study BACE1-substrate interactions at the membrane with substrates such as amyloid precursor protein (APP) and lipoprotein receptor-related protein (LRP).[29,50,53] These earlier studies co-expressed BACE1 with a known substrate, such as APP and LRP, as a labeled FRET pair (GFP-YFP and GFP-Cy3, respectively) as a means to examine the BACE1-substrate interactions at the plasma membrane as indicated by the reduction in the fluorescence lifetimes of the donor molecules.[29,50,53] Their results indicated that LRP was cleaved by BACE1 and that the proximity of APP and BACE1 to each other was increased upon internalization. The authors also reported a fluorescence lifetime of 2.2-2.3 ns for BACE1-EGFP in cultured HEK293 and mouse neuroblastoma (N2a) cell lines, which seems too short when compared with EGFP alone in buffer even after accounting for the refractive index differences.[29] Based on the reported information, such a

disagreement might be attributed to the low signal-to-noise ratio in the previously reported FLIM.[29] To the best of our knowledge, however, the BACE1 dimerization hypothesis has not been investigated using two-photon FLIM. In this chapter and for the first time, we outline our 2P-FLIM results on transfected, adherent HEK cells expressing BACE1-EGFP. These measurements were carried out under untreated and STA-200 inhibited conditions, the latter intended to induce the dimerization of BACE1. In addition, we sampled different expression levels of BACE1-EGFP in our FLIM measurements to minimize the crowding effect of these fusion proteins at the plasma membrane. Care was also taken to rule out any potential two-photon laser-induced photodamage to the cultured cells during 2P-FLIM data acquisition.

4.3 FLIM-Based homo-FRET of BACE1-EGFP: A Dimerization Concept

Fluorescence (or Förster) resonance energy transfer (FRET) is a powerful tool for quantifying intermolecular interactions (e.g., dimer formation) and conformational changes (flexibility) of biomolecules such as proteins and DNA.[52] Based on intermolecular distance ($R_{D\text{-}A}$) between donor (D) and acceptor (A) molecules (FRET pair), the relative orientation of their dipole moment (described by orientation parameter, κ^2), and the spectral overlap between the emission of the donor and absorption of the acceptor, the efficiency of energy transfer (E) between a donor and acceptor may vary according to Eq. 4.1. [54]

$$E = \frac{1}{1+\left(\frac{R_{DA}}{R_0}\right)^6} \quad \text{(Eq. 4.1)}$$

where R_0 is the intermolecular distance between donor and acceptor at which the energy transfer efficiency is 50% (also called Förster distance).[54] This Förster intermolecular donor-acceptor distance (R_0) depends on the spectral overlap between the donor's emission and acceptor's absorption spectra, $J(\lambda)$, the orientation parameter (κ^2), and the refractive index (η) of the surrounding medium such that: [55]

$$R_0^6 \propto \kappa^2 \times J(\lambda) \times \Phi \times \eta^{-4} \quad (4.2)$$

where R_0, κ, $J(\lambda)$, Φ, and η are the donor-acceptor distance, dipole orientation, spectral overlap, chromophore quantum yield, and viscosity of the medium, respectively. For EGFP homoFRET, the estimated R_0 is 4.61 nm,[56] but might be influenced by the size of the tagged protein (BACE1 in our case). FRET efficiency can be determined experimentally using either steady-state spectroscopy or fluorescence lifetime methods.[55] In fluorescence lifetime-based FRET, as used in this thesis project, the energy transfer efficiency (E) can be estimated using the fluorescence lifetime of the free donor (alone without the acceptor, τ_D) and the lifetime of the donor in the presence of the acceptor (τ_{DA}) such that: [55]

$$E = 1 - \frac{\tau_{DA}}{\tau_D} = \frac{1}{1+\left(\frac{R_{DA}}{R_0}\right)^6} \quad (4.3)$$

where E is the energy transfer, τ_D is the fluorescence lifetime of the donor alone in the absence of the acceptor, τ_{DA} is the fluorescence lifetime of the donor in the presence of the acceptor, R_{DA} is the donor-acceptor distance, and R_0 is the Förster distance. Assuming that BACE1-EGFP dimerizes in adherent HEK cells, one may expect a mixed population of monomeric and dimeric fusion proteins (Figure 4.1) throughout the cell. Using FLIM, we should be able to determine the fluorescence lifetime for both monomeric and the potential dimeric populations of BACE1-EGFP throughout the cell with high spatial resolution. Within the spectral overlap region of absorption-emission spectra of BACE1-EGFP, homo-FRET will take place among like molecules that are in a close proximity (with an intermolecular distance up to 10 nm) of each other. For the transmembrane fusion proteins, the 2D restriction of BACE1-EGFP in the membrane will enhance the orientation order and therefore will likely increase the FRET efficiency.[52]

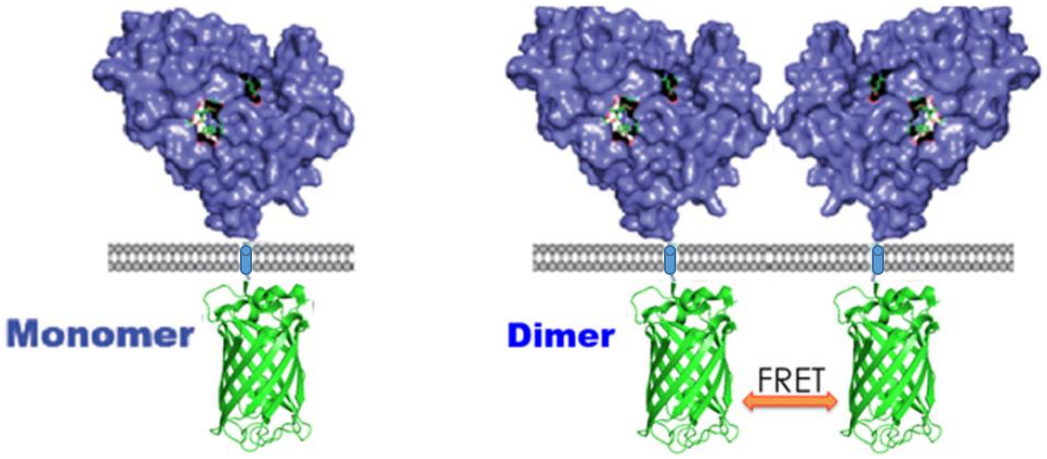

Figure 4.1: Illustration Showing the Potential Monomeric and Dimeric BACE1-EGFP as well as the Corresponding HomoFRET in the Case of a Dimer.

The FLIM image analysis using a frequency-weighted model as a means for testing of the BACE1-EGFP dimerization hypothesis using the homo-FRET (fluorescence resonance energy transfer among a like molecules) approach.[52] To test the dimerization hypothesis, we used the frequency-weighted histogram for each FLIM image to identify any underlying subpopulations (e.g., monomers *versus* dimers). In addition, we also anticipate that the subpopulations of monomeric and dimeric BACE1-EGFP would likely shift under STA-200 inhibition conditions assuming minimal expression of APP in HEK293 cells. Ideally, these measurements will be carried out at different expression levels of the fusion protein in cultured cells in order to differentiate between protein crowding and dimer formation.

4.4 Materials and Methods

Chapter 2 (Materials and Methods) provides a full description of the materials and FLIM methods used for the measurements described here. Briefly, HEK293 cells were cultured to ~80% confluency at which point they were sub-cultured, seeded into 35 mm petri dishes, and incubated. After 24 hours the cells were transfected using Fugene HD^{TM}, a non-liposomal mediated transfection reagent, and incubated 24-48 hours. At least 1 hour prior to measurements, the transfection media was removed and replaced with complete media either with or without the addition of STA-200 inhibitor. 2P-FLIM measurements were carried out using the system depicted in Figure 2.2 (Chapter 2). First, we used confocal microscopy (Figure 2.1, Chapter 2) to locate fluorescent cells and obtain the desired x, y, and z-coordinates. Next, the laser was tuned to pulse 930 nm light at 76 MHz and excite the sample positioned on the microscope stage. Fluorescence emissions were detected, stored, and analyzed as described earlier (Chapter 2).

4.5 Results and Discussion

4.5.1 2P-FLIM of Free EGFP

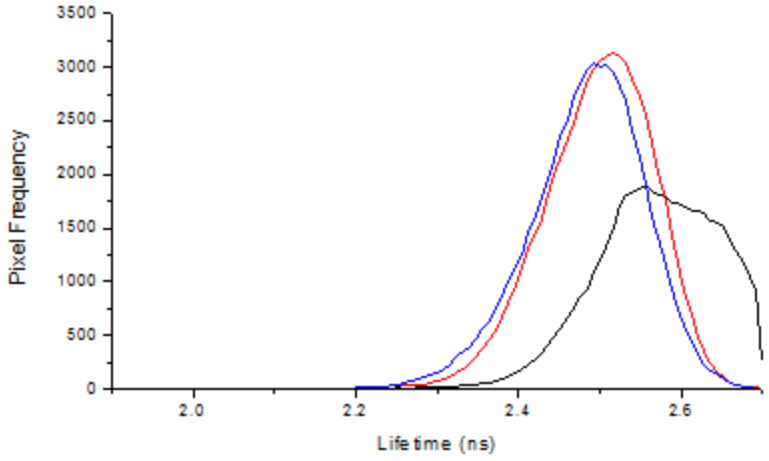

Figure 4.2: 2P-FLIM Histograms of EGFP Solution Studies. Histograms of free EGFP (10 μM) in PBS pH 7.4 (black) and in 2 cP buffered glycerol solution (red) using magic angle detection. In addition, similar measurements were carried out in 2 cP buffered glycerol solution with no magic angle detection (blue).

As a control experiment for our 2P-FLIM of BACE1-EGFP cultured in HEK293 cells, measurements of 10 μM free EGFP were taken in buffered solutions (PBS pH 7.4) as well as in buffered glycerol solution (PBS pH 7.4, 2 cP), consistent with estimated viscosity for cellular cytosol. Histograms of free EGFP averaged over different magnifications (zoom = 3-9) in respective solutions are shown in Figure 4.2. The histogram corresponding to free EGFP in a buffered solution exhibits a relatively wide lifetime distribution centered at ~2.60 ns. EGFP in glycerol solutions (PBS pH 7.4, 2 cP) with and without magic angle detection have lifetime distributions centered at ~2.50 ns. These results show the effect of refractive index (in the glycerol-enriched buffer, 2 cP) on

the mean fluorescence lifetime of EGFP, which resembles that in living cells expressing BACE1-EGFP. Results for both free EGFP in a buffered solutions as well as in 2 cP glycerol solutions are consistent with values found in the literature.[57]

4.5.2 Two-Photon FLIM at Cross-section of Adherent HEK Cells Expressing BACE1-EGFP

We used 2P-FLIM to examine the sensitivities of BACE1-EGFP to its local environment and for potential conformational changes (e.g., dimer formation) in cultured HEK cells under untreated and STA-200 inhibited conditions. A representative cross-sectional 2P-FLIM of HEK cells expressing BACE1-EGFP is shown in Figure 4.2. These representative FLIM images were recorded under untreated (Figure 4.2, top) and STA-200 inhibited (Figure 4.2 bottom) conditions. The corresponding 2P-fluorescence intensity images are also included which, in principle, should provide similar information to the laser-scanning confocal imaging (Chapter 3). In each pixel of the intensity image, the pixel intensity represents the integration of the fluorescence decay in that pixel seen in the corresponding FLIM image, which is as high as up to 8000 counts per pixel at the brightest spot (binning of 2). Such high photon counts per pixel indicate a good signal-to-noise ratio in the corresponding FLIM images. According to our control experiments, the cellular autofluorescence contribution to the 2P-fluorescence and FLIM images reported here (due to such molecules as NADH and flavins)[37] is negligible for 930 nm excitation at the given BACE1-EGFP expression levels in cultured HEK cells.

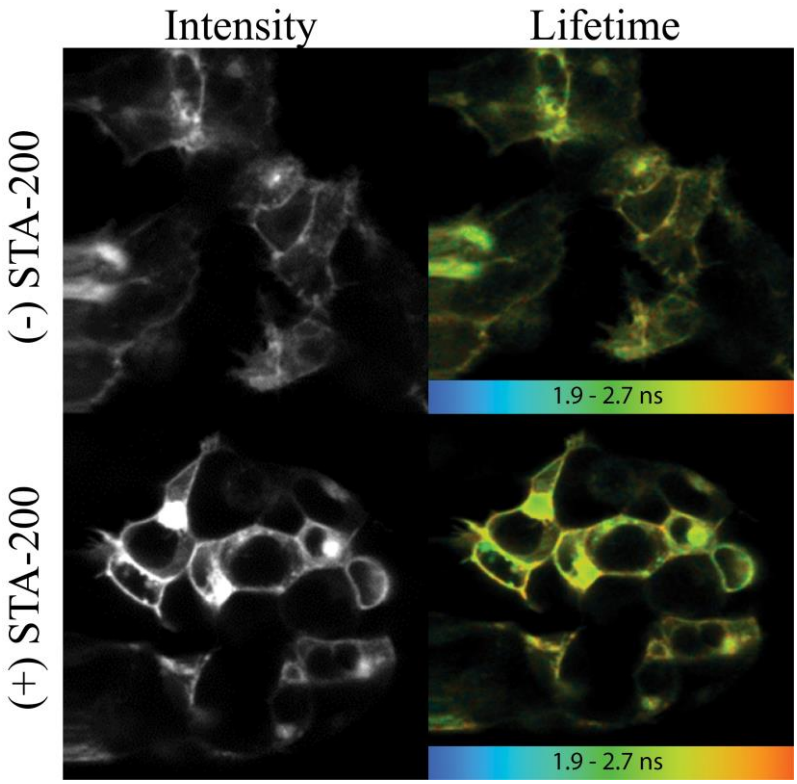

Figure 4.3: Representative Cross-sectional 2P-FLIM Images of HEK293 Cells Expressing BACE1-EGFP. Intensity images (left), fluorescence lifetime images (right), untreated (top), STA-200 inhibited (bottom)

In the absence of STA-200 inhibition (i.e., untreated condition), 2P-FLIM images reveal that the fluorescence decay per pixel (binning of 2) throughout the field of view can be fit satisfactorily with a single exponential decay (Chapter 2: Materials and Methods). However, the frequency-weighted fluorescence lifetime histograms of our BACE1-EGFP FLIM images ($N = 5$) under untreated conditions exhibit a bimodal distribution ranging from 1.9 to 2.7 ns (Figure 4.3).

According to the frequency-weighted fluorescence lifetime histogram (Figure 4.3), one subpopulation of cellular BACE1-EGFP exhibits a mean fluorescence lifetime

of 2.45 ns while another subpopulation has a mean fluorescence lifetime of 2.2 ns (Figure 4.3). The mean 2P-fluorescence lifetime values of BACE1-EGFP are comparable to previous studies where a mean fluorescence lifetime of 2.3 ns was reported.[29] It is hard, however, to compare our FLIM images with those of previous studies due to the lack of published information concerning the signal-to-noise ratio. It is also clear that the measured lifetime of 2.45 ns is relatively shorter than that for free EGFP in a buffer using single-point fluorescence lifetime measurements, where 2.6 ns was reported (Figure 4.2). Such differences can be attributed, in part, to differences in the refractive index for cellular BACE1-EGFP.[57,58] In addition, careful pixel-to-pixel analysis of our FLIM images reveals that the cell membrane bound BACE1-EGFP exhibits a relatively longer fluorescence lifetime compared to its cytosolic counterpart (e.g., in the Golgi apparatus and ER). Remember that EGFP is linked via the C-terminal domain of BACE1 and therefore should sample the cytosolic region nearest to the plasma membrane. This should provide a uniform environment (e.g. temperature, pH, etc.) for BACE1-EGFP and allow any changes in the fluorescence lifetime to be attributed to molecular interactions. With this in mind, these FLIM results suggest dimerization and not heterogeneous conditions.

The histogram of each FLIM image of BACE1-EGFP in cultured HEK cells was analyzed using OriginPro8.1 and fitted with a double Gaussian function such that:

$$f(x) = \left(\frac{1}{\left(2\pi\sigma_1^2\right)^{1/2}}\right) e^{-\left(\frac{(x-a_1)^2}{2\sigma_1^2}\right)} + \left(\frac{1}{\left(2\pi\sigma_2^2\right)^{1/2}}\right) e^{-\left(\frac{(x-a_2)^2}{2\sigma_2^2}\right)} \quad \text{(Eq. 4.4)}$$

where a and σ are the mean and standard deviation, respectively. Figures 4.4 and 4.5 show representative histograms and double Gaussian fitting curves.

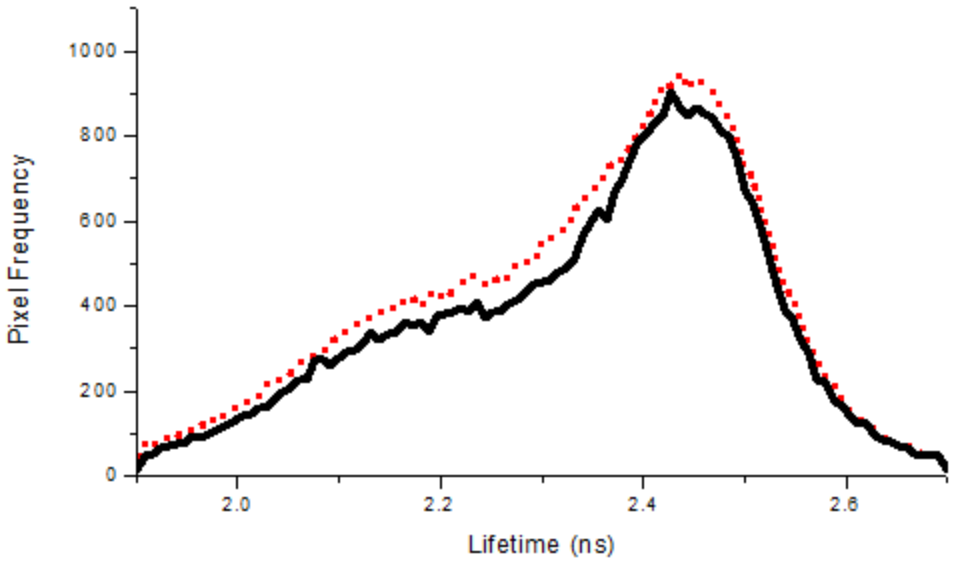

Figure 4.4: Representative Cross-sectional 2P-FLIM Histogram of HEK293 Cell Expressing BACE1-EGFP Untreated conditions (N = 5, dotted), STA-200 inhibited conditions (N = 5, solid)

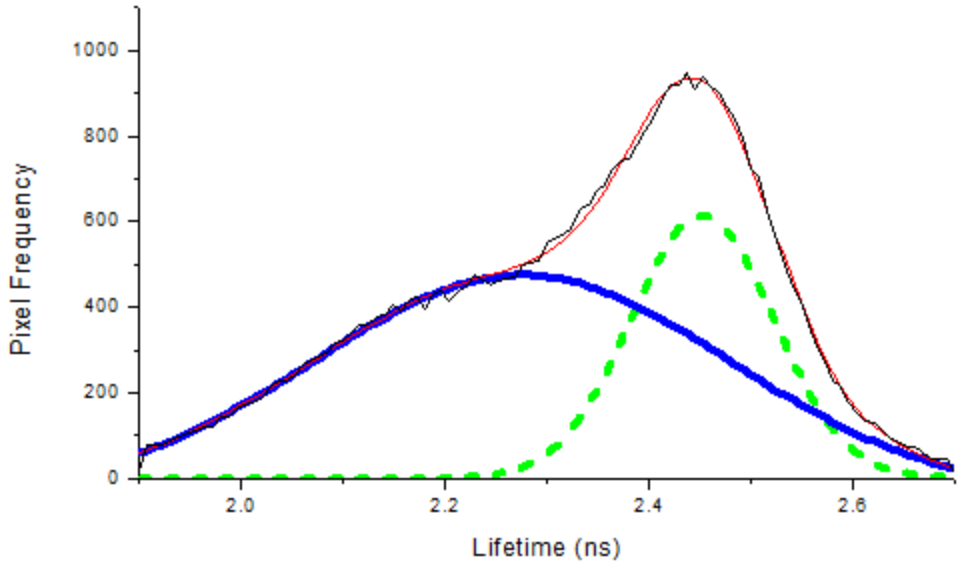

Figure 4.5: Representative Untreated Cross-sectional FLIM Histogram with Double Gaussian Fit. Untreated average (N = 5 cells), peak 1 (solid), peak 2 (dashed)

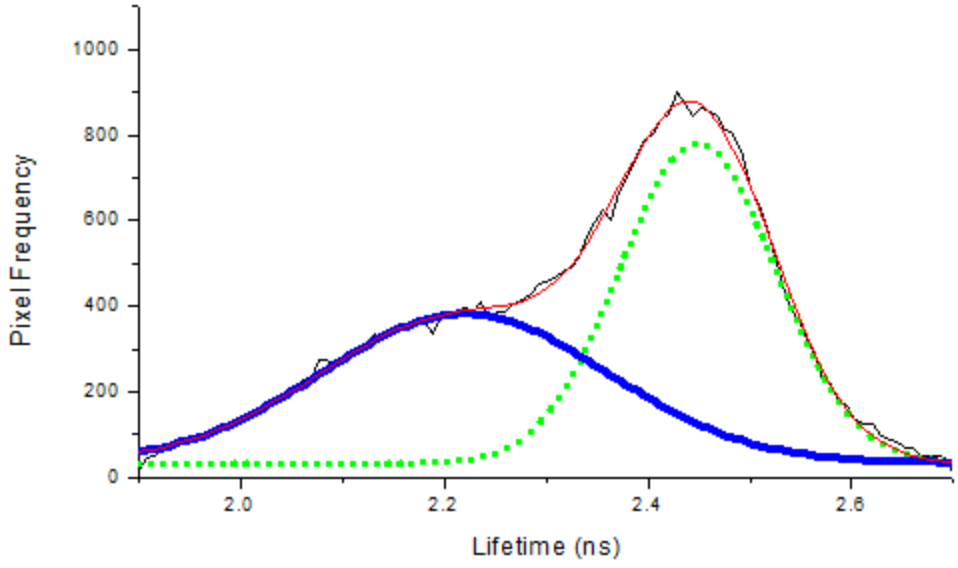

Figure 4.6: Representative STA-200 Cross-sectional FLIM Histogram with Double Gaussian Fit. STA-200 inhibited average (N=5 cells), peak 1 (solid), peak 2 (dashed)

Table 4.1 summarizes the fitting parameters from the double Gaussian fits of the frequency-weighted histograms for the 2P-FLIM images of BACE1-EGFP in HEK cells (N = 10) under untreated and inhibited conditions.

Table 4.1: Fitting Parameters from Double Gaussian Fits of Frequency-weighted Histograms from Cross-sectional FLIM Images. Untreated conditions (N = 5), Inhibited conditions (N = 5), lifetime values are in nanoseconds.

Gaussian Parameters	Untreated Peak 1	Untreated Peak 2	Inhibited Peak 1	Inhibited Peak 2
Peak Center (ns)	$2.28 \pm 5.47 \times 10^{-3}$	$2.45 \pm 9.13 \times 10^{-4}$	$2.22 \pm 6.10 \times 10^{-3}$	$2.45 \pm 1.10 \times 10^{-3}$
Height	526	568	349	750
FWHM (ns)	0.484	0.162	0.332	0.180

Similar 2P-FLIM measurements on cultured HEK cells expressing BACE1-EGFP were recorded under STA-200 inhibited conditions (N = 10). STA-200 inhibits substrate binding to BACE1 by acting as competitive inhibitor and, as a consequence, should facilitate BACE1 dimer formation.[34,36] Representative 2P-FLIM images of STA-200 inhibited HEK cells expressing BACE1-EGFP are shown in Figures 4.2 and 4.6. The cells were incubated with the inhibitor (50 nM) for at least 60 minutes prior to FLIM imaging. The concentration of STA-200 used here is consistent with literature reported conditions.[19] The STA-200 inhibited FLIM images of HEK cells expressing BACE1-EGFP were analyzed as described for untreated cells. This corresponding frequency-weighted histogram (Figure 4.5) also reveals the presence of two populations of BACE1-

EGFP with distinct mean fluorescence lifetime values at 2.2 ns and 2.45 ns. The corresponding double Gaussian fitting parameters are summarized in Table 4.1.

Our analysis of cross-sectional FLIM images indicate that the difference between the frequency-weighted histogram of adherent cells expressing BACE1-EGFP under inhibited and untreated conditions is statistically insignificant ($p>0.05$). Figure 4.3 shows representative FLIM histograms for transfected HEK cells under both untreated and STA-200 inhibited conditions ($N = 5$).

To quantitatively assess these histograms under STA-200 inhibited conditions, the two Gaussian distributions functions were fit using Origin 8.1 peak fitting software to calculate FWHM (Figure 4.5). Relevant fitting parameters for these distributions are shown above in Table 4.1.

The Gaussian fitting suggests that there are two populations of BACE1-EGFP, which are subject to different local environments. One possible explanation for the appearance of two populations could be homoFRET. If homoFRET is occurring in a subpopulation of BACE1-EGFP, the fluorescence lifetimes would be considerably shorter compared to BACE1-EGFP subpopulations not experiencing homoFRET. This could be due to dimerization, which would bring two BACE1-EGFP molecules well within the Förster distance, allowing homoFRET to occur. There are a couple of possible reasons why STA-200 inhibition seemed to have no effect on the change in the two lifetime distributions. It is possible that STA-200 has low cell permeability and therefore does not have access to the intracellular BACE1-EGFP that is responsible for a major portion of cross-sectional fluorescent lifetimes. Another possibility is that intracellular

BACE1-EGFP is already in a dimer complex with very low amounts of endogenous substrate present and therefore not affected, to a noticeable degree, by STA-200 inhibition.[59]

4.5.3 FLIM at the Cell Surface-Glass Coverslip Interface Reveals Two Fluorescence Lifetime subpopulations, which are Dependent on Inhibition by STA-200

To gain further insight into the effects of local environment on BACE1-EGFP expressed in HEK293 cells, we carried out 2P-FLIM measurements at the cell surface-glass coverslip interface. As stated previously, BACE1 does not co-localize with endogenous substrate, such as APP, until endocytosis from the plasma membrane occurs.[50] Once internalized into acidic compartments, BACE1 activity increases facilitating cleavage of protein substrates.[16,22] Since dimerization has been suggested to be mediated by substrate binding, FLIM measurements were performed on the cell surface-glass interface under untreated and STA-200 inhibited conditions.[34,36] Figure 4.6 contains both fluorescence intensity and corresponding fluorescence lifetime images from these measurements. Images taken at the cell surface, as with those taken at the cross-section, align relatively well with lifetimes for BACE1-EGFP that have previously have been reported in the literature (2.3 ns).[29] The fluorescence lifetime images in Figure 4.6 show, similar to Figure 4.2, a wide distribution of fluorescence lifetimes.

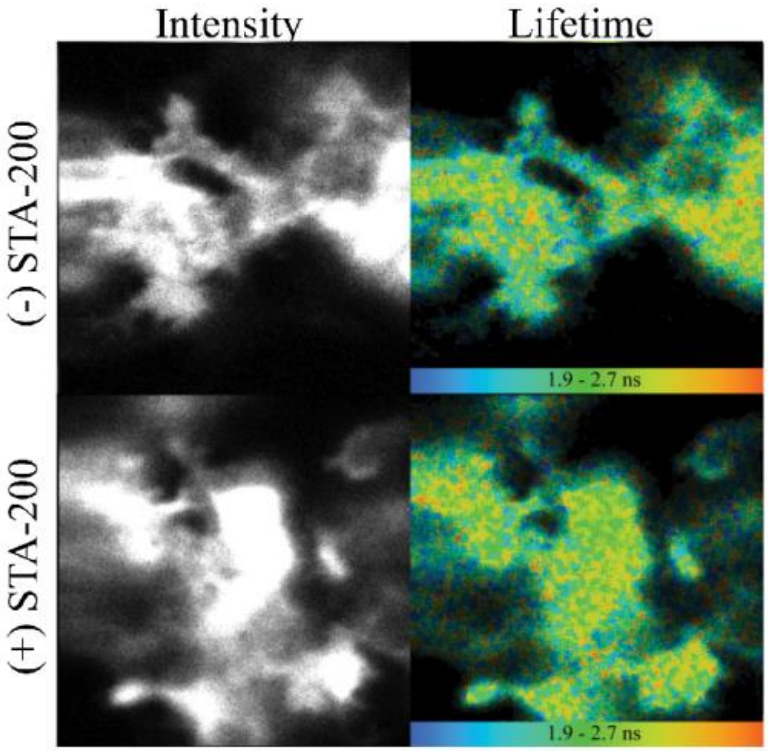

Figure 4.7: Representative 2P-FLIM Images at the Cell Surface-Glass Coverslip Interface of HEK293 Cells Expressing BACE1-EGFP. Intensity images (left), fluorescence lifetime images (right), untreated (top), STA-200 inhibited (bottom)

The pixel frequency histogram for these color-coded values can be seen in Figure 4.7, which shows representative distributions under both untreated (dotted) and STA-200 inhibited (solid) conditions. At first glance it seems that not only are two lifetimes present, but that there is also a difference in the lifetime distributions between the inhibited and untreated states.

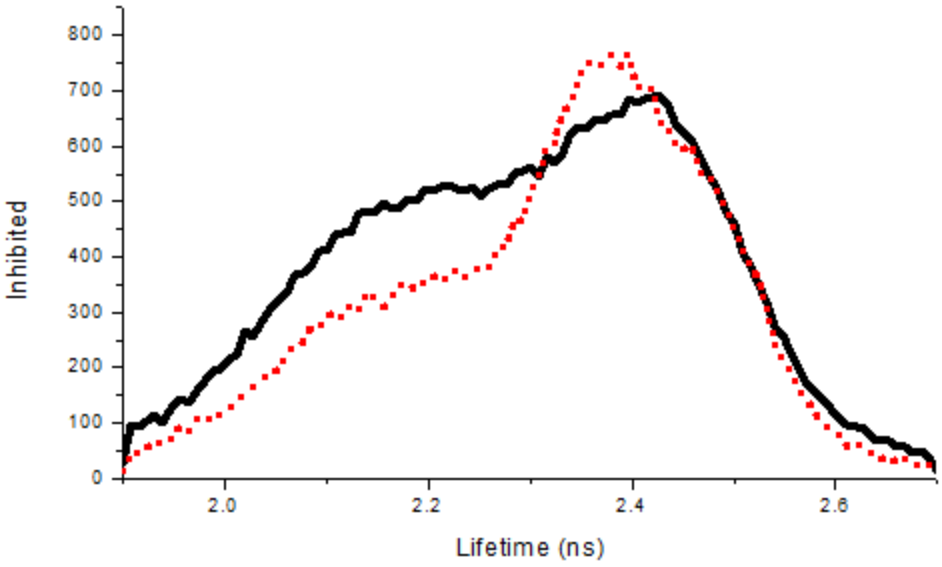

Figure 4.8: Representative Histogram of 2P-FLIM at Cell Surface-Glass Coverslip Interface. Untreated conditions (N = 5, dotted), STA-200 inhibited conditions (N = 5, solid).

To help quantify the difference in the distributions, we fit the individual histogram representing untreated or inhibited conditions to a double Gaussian function using the Origin 8.1 software (Figure 4.8 and 4.9). The fitting parameters from the double Gaussian fits of these distributions are provided in Table 4.2. From the figure and table it is clear that there is a shift in the relative magnitude of the two fluorescence lifetime subpopulations with the longer lifetime subpopulation decreasing in size with a corresponding increase in size of the shorter lifetime subpopulation. As stated previously, the centers of these distributions coincide well with acceptable lifetimes for BACE1-EGFP, but it is important to note that the longer lifetime of 2.4 ns is consistent with the literature values for the expression of monomeric BACE1-EGFP, while the distribution centered at 2.1 ns is very close to the expected lifetime of BACE1-EGFP co-expressing substrate containing a FRET acceptor.[50] In light of this, it is reasonable to infer that

BACE1-EGFP is acting as both a donor and acceptor (homoFRET). Also, when the environment of BACE1-EGFP is altered by the addition of the STA-200 inhibitor, there is an apparent increase in the FWHM for the subpopulation with the shorter fluorescence lifetime. This could be a result of substrate-mediated dimerization as proposed by the groups of Multhaup and Lendahl.[34,36] The difference in fluorescence lifetime histograms between the cross-sectional and cell surface images can be explained by the fact that BACE1 and an endogenous substrate (such as APP) are not in close proximity on the cell surface but are located near one another following endocytosis.[50] Therefore it would be reasonable to speculate that intracellular BACE1-EGFP could be in complex with substrate, while BACE1-EGFP on the cell surface is not until the addition of the transition state analog inhibitor STA-200.

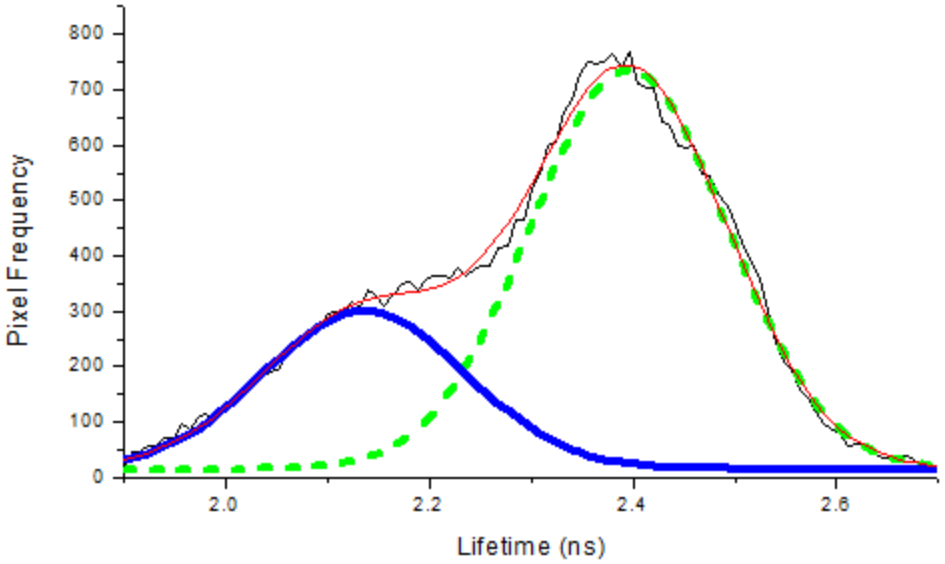

Figure 4.9: Representative Cell Surface-Glass Coverslip Interface FLIM Histogram Fitted to a Double-Gaussian Function. Untreated average (N=5 cells), peak 1 (solid), peak 2 (dashed).

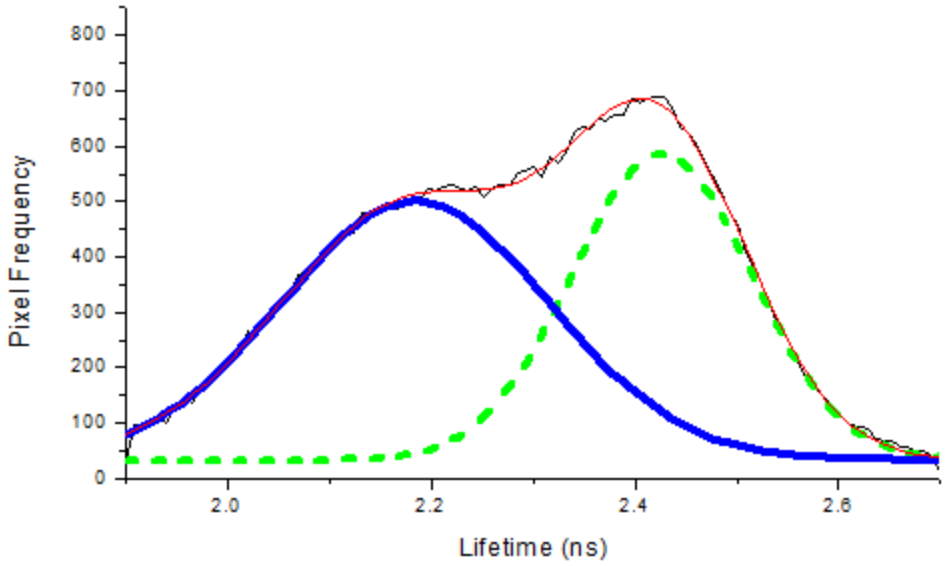

Figure 4.10: Representative Cell Surface-Glass Coverslip Interface FLIM Histogram Fitted to a Double-Gaussian Function. STA-200 inhibited average (N = 5 cells), peak 1 (solid), peak 2 (dashed).

Table 4.2: Fitting Parameters for Double Gaussian Fits of Fluorescence Lifetime Histograms from Cell Surface 2P-FLIM Images. Untreated conditions (N = 5), STA-200 inhibited conditions (N = 5), lifetime values are in nanoseconds.

	Untreated Peak 1	**Untreated Peak 2**	**Inhibited Peak 1**	**Inhibited Peak 2**
Peak Center (ns)	2.136 ± 0.005	2.396 ± 0.002	2.184 ± 0.003	2.426 ±0.001
Height	284	720	468	553
FWHM (ns)	0.234	0.228	0.311	0.208

Table 4.3: Area of Fitted Gaussian Lifetime Distributions. N = 5 for cross-section and cell surface glass interface under respective conditions.

	Untreated Peak 1	**Untreated Peak 2**	**Inhibited Peak 1**	**Inhibited Peak 2**
Cross-section	$2.22 \times 10^5 \pm 1.40 \times 10^4$	$1.34 \times 10^5 \pm 4.18 \times 10^4$	$2.06 \times 10^5 \pm 1.08 \times 10^5$	$2.11 \times 10^5 \pm 2.60 \times 10^4$
Cell Surface	$1.75 \times 10^5 \pm 7.26 \times 10^4$	$1.29 \times 10^5 \pm 4.97 \times 10^4$	$1.71 \times 10^5 \pm 2.43 \times 10^4$	$1.48 \times 10^5 \pm 3.45 \times 10^4$

Statistical analysis of the area under each Gaussian curve revealed no difference (p-value > 0.05) between untreated and STA-200 inhibited conditions. Despite this fact, there appears to be a trend involving STA-200 inhibition and a shift to the subpopulation with the shorter lifetime (Figure 4.7). A lack of statistical significance is most likely due to small sample size or lack of an effect due to STA-200. For future experiments FLIM images at the cell membrane-glass interface should exceed sample sizes of at least fifteen. In addition, the experiments should be conducted at various STA-200 concentrations to ascertain whether the observed modest change is dose-dependent.

Using FRET analysis (Eq. 4.3) above, FRET efficiency (E) was found to be 7% and 10% for BACE1-EGFP homoFRET based on lifetimes from cross-sectional images for uninhibited and inhibited conditions, respectively. FRET efficiency for the cell surface measurements were 12% and 11% for uninhibited and inhibited, respectively Based on this, the intermolecular distance (R_{DA}) was found to be 6.4-7.1 nm assuming a Förster distance of 4.61 nm.[60]

4.6 Conclusions

To test the dimerization hypothesis of BACE1, we used 2P-FLIM to gain a better understanding of the sensitivities of BACE1-EGFP to conformational and environmental changes in living cells. Pixel-by-pixel analyses of cross-sectional FLIM images reveal collectively longer lifetimes on the membrane when compared to internal compartments such as the Golgi apparatus. Analysis of pixel frequency weighted histograms indicated the presence of multiple BACE1-EGFP lifetime distributions. The corresponding FLIM histograms, recorded at both the cross-section of the cell as well as at the cell surface-glass coverslip interface under untreated and STA200 inhibited conditions, were analyzed using to a double-Gaussian function. Such analyses revealed a shift in the subpopulations corresponding to two distinct fluorescence lifetimes and make inferences concerning local interactions. Namely, we were able to show the presence of two subpopulations with lifetimes centered at 2.1 ns and 2.4 ns, possibly due to the subpopulation of dimeric BACE1-EGFP with the shorter fluorescence lifetime undergoing homoFRET as

compared with monomeric subpopulation. In addition, FRET analysis indicated an energy transfer efficiency (E) to be 7-11% with an estimated donor-acceptor distance of R_{DA} = 6.4-7.1 nm. Also in studies regarding the cell surface-glass coverslip interface with the addition of the STA-200 inhibitor, we observed a trend in which the subpopulation with a fluorescence lifetime around 2.1 ns increased, while the subpopulation centered around a fluorescence lifetime of 2.4 ns seemed to decrease. Although this apparent change in subpopulations contributing to the overall fluorescence lifetime distribution is not statistically significant (p-value > 0.05), performing dose-dependent STA-200 studies and increasing the sample size may further elucidate effects of STA-200 inhibition on BACE1-EGFP fluorescence lifetimes. With that being said, the next question that needed to be answered was: is the rotation of BACE1-EGFP on the nanosecond timescale consistent with that of the monomeric or dimeric form of BACE1-EGFP? To answer this question we turned to time-resolved anisotropy measurements on our model system.

Chapter 5

Nanosecond Conformational Flexibility of BACE1-EGFP in HEK293 Cells

5.1 Summary

Detergent-based studies have suggested that BACE1 forms dimers. In this chapter, we examine the rotational motion and flexibility of BACE1-EGFP in adherent HEK293 cells using a noninvasive, quantitative trFA method. In these studies, cells expressing BACE1-EGFP were excited using one-photon (465 nm) pulses (~120 fs, 4.2 MHz) under both untreated and STA-200 inhibited conditions. Our results indicate that the fluorescence anisotropy of BACE1-EGFP decays as a biexponential with a fast rotational time (~1 ns, amplitude = 0.07) and a slow component (~17 ns, amplitude = 0.21) under untreated conditions. The first rotational component is too fast to be assigned as a segmental motion of the EGFP in BACE1-EGFP construct within the cytosolic proximity of the plasma membrane in adherent HEK cells. As a result, we attributed this fast component to homo-FRET between BACE1-EGFP units in a homodimer. In contrast, the slow rotational decay component (28-40 ns) seems sensitive to both intracellular location (plasma membrane *versus* Golgi apparatus) and inhibition by STA-200. These nanosecond rotational dynamic studies on HEK cells expressing BACE1-EGFP complement our FLIM studies (Chapter 4) and provide new insights into the conformational flexibility and association of BACE1-EGFP noninvasively under physiological conditions.

5.2 Background

1P-trFA is a powerful approach for investigating fast rotational motion, association, and conformational flexibility of biomolecules in different environments.[61] There are different modalities of anisotropy measurements that can be employed to answer specific questions for a given molecular process and its surrounding environment. For example, steady-state anisotropy methods and anisotropy imaging microscopy are used to investigate a wide range of protein conformational changes.[61] In addition, time-resolved anisotropy provide real-time dynamics associated with structural changes and conformational flexibility.[61]

Time-resolved anisotropy, on the other hand, has been used previously to determine levels of aggregation for a multitude of proteins.[62] Specifically, the same approach proved useful in investigating energy transfer among the building blocks of those protein aggregates based on homoFRET (fluorescence resonance energy transfer between like molecules).[62] For example, recent dimerization studies on the amyloid precursor protein (APP) have been reported using time-resolved anisotropy measurements and homoFRET analysis in a cultured HEK293 cell line.[63] In those studies, the authors used HEK293 cells to express APP tagged with EGFP to show that homoFRET occurred under physiological conditions.[63] In addition, the rate of homoFRET between proteins was assigned to an apparent <8 ns rotational component in the anisotropy decay curve.[63] To the best of our knowledge, however, the application of this approach to test the dimerization hypothesis of BACE1 in living cells has not been reported.

In this chapter we show 1P-trFA measurements on adherent HEK cells expressing BACE1-EGFP under untreated and STA-200 inhibited conditions. Our trFA is based on the time-correlated single-photon counting technique as described in Chapter 2 (Materials and Methods).[39] These measurements were carried out where the 1P laser pulses (465 nm, ~120 fs, 4.2. MHz) were randomly focused on different locations within the plasma membrane and Golgi apparatus. The results were analyzed and modeled to test the hypothesis of BACE1-EGFP dimerization as well as to assess the structural flexibility of this fusion protein in different intracellular compartments.

5.3 Materials and Methods

For a full description of materials and methods used herein, please refer to Chapter 2. Briefly, HEK293 cells were cultured to ~80% confluency at which point they were sub-cultured, seeded into 35 mm petri dishes, and incubated. After 24 hours, the cells were transiently transfected using Fugene HD^{TM}, a non-liposomal mediated transfection reagent, and incubated for 24-48 hours. At least 1 hour prior to taking measurements, the transfection media was removed and replaced with complete media either with or without the addition of STA-200 inhibitor (50 nM final concentration). For 1P-trFA, 465-nm laser pulses (~120 fs, 4.2 MHz) were used as described in Figure 2.2 (Chapter 2). The laser pulses were randomly focused on different locations inside the cultured HEK cells to sample BACE1-EGFP in the plasma membrane and the Golgi apparatus under untreated and STA-200 inhibited conditions. These measurements were

repeated on different cells, dishes, and days to ensure the reproducibility of our results and to avoid systematic errors.

5.4 Results and Discussion

5.4.1 Calibration of Our Time-Resolved Anisotropy Setup

Following the careful alignment of our 465-nm excitation pulses through the back-exit of our inverted microscope, time-resolved anisotropy of Rhodamine Green (RhG; 2.0 μM) was measured in an aqueous droplet (PBS, pH 7.4) on a glass coverslip at room temperature. The time-resolved parallel and perpendicular fluorescence polarizations were recorded using SPC-830 module (Chapter 2), formatted using SPCImage, and analyzed using OriginPro software. It is worth noting that the parallel and perpendicular fluorescence polarization decays were collected simultaneously (using T-configuration) to rule out any fluctuation in the excitation laser intensity during the anisotropy decay measurements. The geometrical factor (or G-factor) of our experimental setup was determined using tail-matching approach with an estimated *G*-value of 0.612.[37] The corresponding anisotropy decays for RhG was then calculated from the parallel and perpendicular fluorescence polarization decays with a rotational time of 160 ± 5 ps (see Figure 5.2 for a typical representative anisotropy decay for RhG). As mentioned in Chapter 2, OriginPro8.1 software and non-linear least squares fitting algorithms were used to fit the observed anisotropy decays. The measured rotational time is consistent with the volume of RhG in a buffer at room temperature. The measured rotational time is also consistent with literature values for such a small fluorophore at

room temperature.[64] This calibration was carried out twice during the course of daily experiments (at the beginning and at the end of the measurements).

As a control, 1P-trFA measurements were collected for 10 μM free EGFP in buffer (PBS pH 7.4, ~1 cP) and in buffered glycerol solution (PBS pH 7.4, η = 2 cP) to simulate rotation in a viscous environment comparable to the cell cytosol. Anisotropy measurements of these samples reveal free EGFP has rotational times of 29.3 ± 3.0 ns and 51.0 ± 1.5 ns for EGFP in buffer and in buffered glycerol solution, respectively.

Once the system was calibrated, the same experimental conditions were maintained during the whole set of measurements on HEK cells expressing BACE1-EGFP. The only exception was the excitation laser intensity, which was varied based on the expression level to ensure a good signal-to-noise ratio for the measured anisotropy decays. In addition, the laser beam was focused randomly on different locations inside the HEK cells expressing BACE1-EGFP, most likely the plasma membrane and the Golgi apparatus (Figure 5.1).

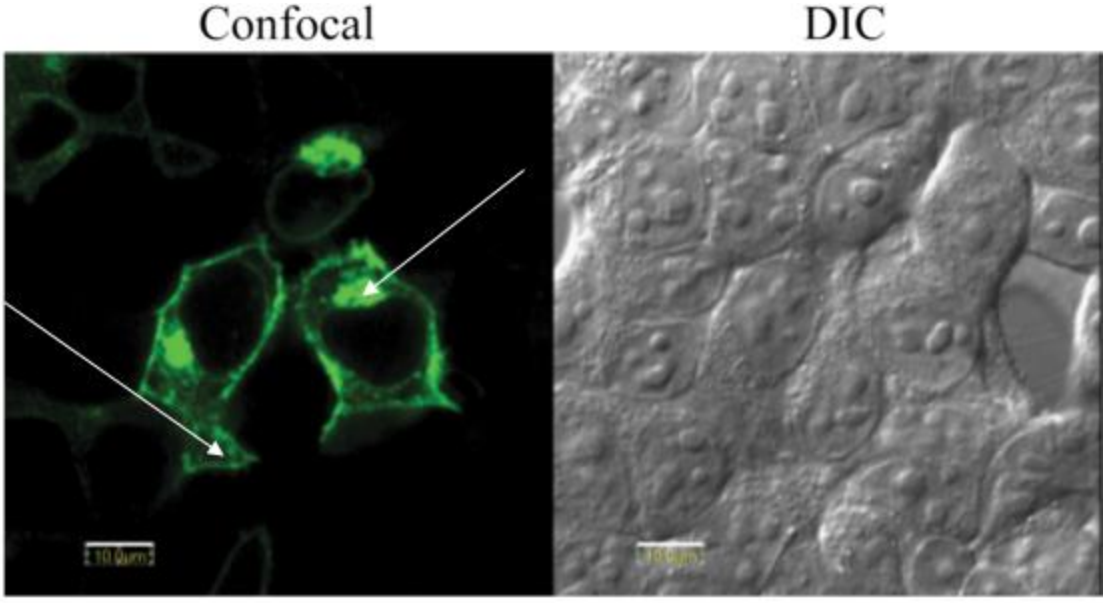

Figure 5.1: Locations of 1P-trFA in HEK293 Cells Expressing BACE1-EGFP. Confocal (left), DIC (right), arrows indicate representative cellular locations of 1P-trFA measurements.

5.4.2 Rotational Diffusion of BACE1-EGFP on the Plasma Membrane of Cultured HEK Cells

We used the calibrated 1P-trFA measurements to examine the structural flexibility and conformation of BACE1-EGFP in HEK293 cells under untreated conditions at room temperature. For our measurements we used confocal and DIC imaging to selectively position the second harmonic generated laser pulses (465 nm, ~120 fs, 4.2 MHz) either on the cell membrane near the periphery of the cell where the bilayers are collapsed or on an internal compartment (the apparent trans-Golgi network). The fluorescence signal was stable during the course of the fluorescence polarization measurements (3 minutes per polarization-analyzed curve with a maximum of 60,000 photons). For statistical analysis,

these measurements were repeated (N = 41 total) using different cells, dishes, and days of experiments to ensure reproducibility, assess the standard deviation in our measurements, and to avoid systematic errors.

Representative anisotropy decays of BACE1-EGFP on the plasma membrane of cultured, untreated HEK cells are shown in Figure 5.2. The anisotropy curves of BACE1-EGFP in the plasma membrane (Figure 5.2, Curves 2 and 4) were analyzed using biexponential decay functions (Equation 2.3, Chapter 2: Materials and Methods) with a least-squares fitting routine (Origin 8.1 non-linear regression software). A representative anisotropy decay of RhG under the same experimental conditions and on the same time scale is shown for visual comparison (Figure 5.2, Curve 1).

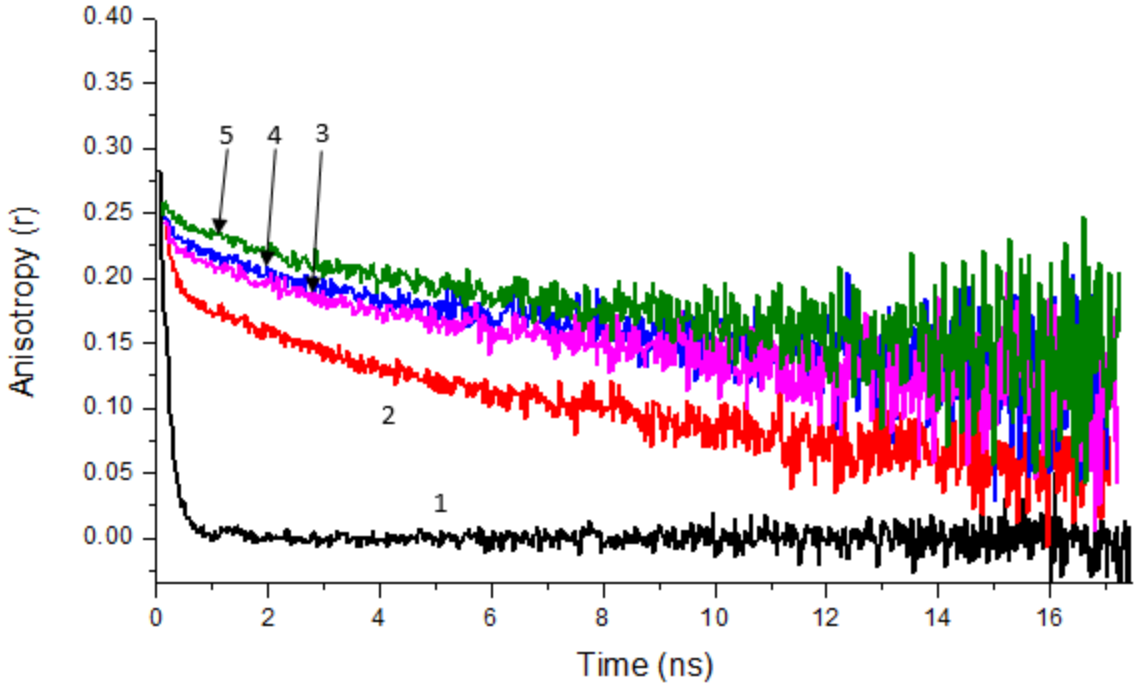

Figure 5.2: Representative Anisotropy Curve of HEK932 Cells Expressing BACE1-EGFP. 1) Rhodamine Green, 2) Untreated Plasma Membrane, 3) Untreated Golgi apparatus, 4) Inhibited Plasma Membrane, 5) Inhibited Golgi apparatus. The biexponential fitting parameters (see Equation 2.3, Chapter 2) for the anisotropy decays are summarized in Table 5.1 and Table 5.2 for measurements on different cellular compartments.

The fitting parameters for the anisotropy decay curves of BACE1-EGFP on the plasma membrane and within internal compartments of the cultured HEK cells are summarized in Table 5.1 (plasma membrane) and Table 5.2 (intracellular compartments, which is likely the Golgi apparatus).[24] The fitting parameters of the single-exponential anisotropy decay of RhG in buffer at room temperature are also included for comparison. To examine whether the fitting parameters of BACE1-EGFP rotational motion in the plasma membrane were significantly different, we carried out Welsh's *t*-test analysis.[63] It is worth noting that the Welsh's *t*-test is not skewed by unequal population size of measurements or inequivalent variance for each group. The corresponding *p*-values in

Welsh's *t*-test analysis are also shown in Table 5.1, with the *p*-value < 0.05, this is an indication of no statistical difference between the means for each group of measurements.

Table 5.1: Fitting Parameters for Anisotropy Curves of HEK293 Cells Expressing BACE1-EGFP in the Plasma Membrane Under Both Untreated and STA-200 Inhibited Conditions. Parameters from the biexponential anisotropy decay fits, amplitude (β) and rotational time (ϕ), for each condition are shown. The calculated standard deviation and the estimated *p*-values in the Welsh's *t*-test are also shown.

Plasma Membrane	Untreated (N = 10)	Inhibited[a] N = 11)	*p*-value
β_1	0.07 ± 0.03	0.04 ± 0.01	0.062
ϕ_1 (ns)	0.40 ± 0.26	1.4 ± 0.9	0.0085
β_2	0.21 ± 0.02	0.21 ± 0.02	0.61
ϕ_2 (ns)	17 ± 4	28 ± 7	0.0010

[a] Cells expressing BACE1-EGFP were inhibited using STA-200 (50 nM, 60 minutes incubation)

The fast component (ϕ = 0.40 ± 0.26 ns) of BACE1-EGFP (β = 0.07 ± 0.03) under untreated conditions seems too fast as compared with the rotational time of free EGFP in a cell (~10 ns).[56] As a result, we attribute the fast anisotropy decay component of BACE1-EGFP to homo-FRET between a dimeric pair on the plasma membrane. This assignment of the fast rotational component of our fusion protein is consistent with literature studies on APP-EGFP in a HEK293 cell line using a similar experimental approach.[63] In addition, our results suggest that the STA-200 inhibition has a significant (p = 0.0085) effect on the fast rotational time of BACE1-EGFP (Table 5.1). Such

sensitivity to STA-200 inhibition is also consistent with our assignment of the fast rotational component as a fingerprint of homo-FRET.

Our results also show that the slow rotational time (17 ± 4 ns) of BACE1-EGFP on the plasma membrane of HEK cells under untreated conditions is slightly faster than that of free EGFP (~29 ns) in pure buffer at room temperature. Such a difference in the rotational mobility can be understood in terms on the membrane restriction imposed on the EGFP at the C-terminus of the BACE1 protein. Assuming the BACE1-EGFP protein to be ~105 kDa with a degree of hydration of 5 nm, the expected rotational time as a sphere in buffer using Eq. 2.4 (chapter 2) should be ~110 ns. In addition, the cytosolic viscosity in the vicinity of the plasma membrane must be considered to slow down the tumbling motion of the EGFP moiety of the fusion protein. Our results also indicate that the slow rotational motion of BACE1-EGFP is sensitive to STA-200 inhibition with an estimated rotational time of $\phi_2 = 28 \pm 7$, the differences are statistically significant ($p = 0.0010$). Based upon these results it is possible that the increased rotational time is due to internalization of STA-200 inhibited BACE1-EGFP, but considering that the rotational time approximately doubles, it seems unlikely that this event is due to a process other than dimerization.

The initial anisotropy ($r_0 = 0.271$) of BACE1-EGFP expressed in the plasma membrane on HEK cells is less than the theoretical limit for 1P-anisotropy measurements (0.4). It is worth mentioning that the initial anisotropy is related to the angle between the absorbing and emitting dipole of the rotating fluorophore (EGFP in this case).[61] This observation is in a close agreement with the studies of Devauges *et al.* on the rotational

mobility of APP in HEK293 cells.[63] Such an observation can be attributed to a fast non-radiative (or undetectable) dynamic process of BACE1-EGFP on a faster timescale below our temporal resolution. STA-200 inhibition of BACE1-EGFP seems to affect the initial anisotropy (0.245) as compared with the untreated conditions (p-value < 0.05)

5.4.3 Rotational Diffusion of Intracellularly Expressed BACE1-EGFP (Golgi Apparatus) of Cultured HEK Cells

Similar anisotropy measurements were carried out on internally trafficked BACE1-EGFP in the Golgi apparatus. Representative 1P-anisotropy curves are shown in Figure 5.2 under both untreated and STA-200 inhibited HEK cells. Using the same data analysis approach described above, the corresponding fitting parameters are summarized in Table 5.2.

Table 5.2: Fitting Parameters for Anisotropy Curves of Intracellularly Compartmentalized BACE1-EGFP in HEK293 Cells Under Both Untreated and STA-200 Inhibited Conditions. The parameters from the biexponential anisotropy decay fits, amplitude (β) and rotational time (ϕ), for each condition are shown. The calculated standard deviations and the estimated *p*-values in the Welsh's *t*-test are also shown.

Intracellular Compartment[a]	Untreated (N = 10)	Inhibited[b] (N = 10)	*p*-value
β_1	0.040 ± 0.013	0.050 ± 0.016	0.14
ϕ_1 (ns)	1.3 ± 0.7	2.3 ± 1.05	0.013
β_2	0.21 ± 0.03	0.20 ± 0.03	0.28
ϕ_2 (ns)	31 ± 5	40 ± 13	0.14

[a] Apparent Golgi apparatus as shown in the confocal images in Chapter 3

[b] Cells expressing BACE1-EGFP were inhibited using STA-200 (50 nM, 60 minute incubation)

Interestingly, the results suggest that the anisotropy decay of BACE1-EGFP in the Golgi apparatus also decays as a biexponential with a fast rotational time of 1.3 ± 0.7 ns as compared with a slow rotation of 31 ± 5 ns under untreated conditions (Table 5.2). Our Walsh's *t*-test analyses indicate that the differences in amplitude fractions (β_1 and β_2) and the slow rotational component (ϕ_2) are statistically insignificant ($p > 0.05$) under STA-200 inhibited conditions (Table 5.2). However, the results suggest that the fast rotational time of BACE1-EGFP is significantly ($p = 0.013$) slower (2.3 ± 1.0 ns) under STA-200 inhibited conditions as compared with that under untreated conditions (Table 5.2). This can be attributed to enhanced homo-FRET efficiencies under untreated conditions, which is consistent with our understanding of STA-200 inhibition of BACE1. Evidence from the literature reveals that increased homoFRET should cause further

depolarization of EGFP, resulting in faster rotational times.[63] As we see in Table 5.2, the fast rotational time for STA-200 inhibited conditions is slower than untreated. An explanation could be a change in local viscosity but since no difference was observed for the slow rotating species, this seems unlikely. A rationale for the lack of a difference between the slow diffusing species under different conditions could be due to low amounts of endogenous substrate, such as APP, facilitating dimerization by being in close proximity intracellularly.[34,36] Considering the role of STA-200 in our experiment is to induce dimerization in HEK293 cells expressing BACE1-EGFP, it seems probable that endogenous substrate may cause some interference.

Comparison of Table 5.1 (plasma membrane) and Table 5.2 (Golgi apparatus) also suggests that the rotational times (both fast and slow components) of BACE1-EGFP in the Golgi apparatus of HEK cells is significantly slower than that in the plasma membrane. These results indicate potential environmental differences and conformations associated with the location of BACE1-EGFP in the adherent HEK cell line. This could be a result of local viscosity changes in the plasma membrane and Golgi apparatus. An additional explanation could be that BACE1-EGFP dimers in the Golgi apparatus are complexed with endogenous transmembrane substrates such as the APP which would hinder the rotation of EGFP attached to the C-terminus of BACE1.[59] Membrane-bound BACE1-EGFP dimers would be complexed with STA-200 and so the attached EGFP would not be hindered.

The longer rotational time (20-35 ns) is more consistent with what would be expected for EGFP alone in the labeled fusion protein construct in cytosol, yet this

rotational time is still much shorter than what would be expected for a transmembrane protein (~80 ns).[63] For our BACE1-EGFP there is the large catalytic N-terminal domain, single-transmembrane domain, and short C-terminal domain, which is connected to EGFP through a 12 amino acid linker. In short, this structure is two rigid portions (EGFP and the catalytic/transmembrane domain) connected through a flexible linker. Studies of such proteins have yielded anisotropy values that are smaller than what is expected due to short segmental motion, illustrated below in Figure 5.3.[56]

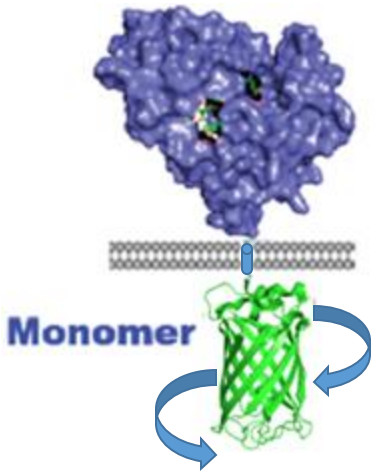

Figure 5.3: Illustration Illustrating the Fast Segmental Motion of BACE1-EGFP.

5.4.4 Apparent Hydrodynamic Radius Calculations of Rotating Fusion Protein

To further investigate the size differences between the rotating species of BACE1-EGFP, Welsh's *t*-tests (Tables 5.1 and 5.2) were carried out to calculate the corresponding apparent hydrodynamic radii (a_{app}) (Table 5.3) under untreated or STA-200 inhibited conditions in adherent HEK cells. In these calculations, we used the slow rotational time component to assess the global mobility of BACE1-EGFP species in the plasma membrane of HEK cells under different physiological conditions, assuming a membrane-like viscosity (4.5 cP).[65]

Table 5.3: Rotational Diffusion Coefficients and Apparent Hydrodynamic Radii of BACE1-EGFP in an Internal Compartment or on the Plasma Membrane

	D_R (s^{-1})[a]	a_{app} (nm)[b]
(A) Plasma Membrane:		
$\phi_{2\ \text{untreated}}$	0.011 ± 0.002	1.5 ± 0.1
$\phi_{2\ \text{inhibited}}$	$6.0 \times 10^{-3} \pm 1.8 \times 10^{-3}$	1.81 ± 0.16
(B) Internal Compartment:		
$\phi_{2\ \text{untreated}}$	$5.0 \times 10^{-3} \pm 8.6 \times 10^{-4}$	1.87 ± 0.10
$\phi_{2\ \text{inhibited}}$	$5.0 \times 10^{-3} \pm 1.3 \times 10^{-3}$	2.0 ± 0.2

[a] *The rotational diffusion coefficient (D_R) was calculated using Equation 2.4.1*

[b] *The apparent radius of the rotating moiety (a_{app}) was calculated using Equation 2.4 and the equation for volume of a sphere.*

Table 5.4: Statistics on Mean Values of Apparent Hydrodynamic Radius of BACE1-EGFP in Indicated Cellular Locations (*p*-values were obtained using Welsh's *t*-test, with the null hypothesis being no statistical difference between group means.)

	***p*-value (*t*-test)**
(A) Plasma Membrane (PM)	
$a_{2\ \text{untreated}}$(PM) vs. $a_{2\ \text{inhibited}}$ (PM)	1.3×10^{-4}
(B) Internal Compartment (IC)	
$a_{2\ \text{untreated}}$ (IC) vs. $a_{2\ \text{inhibited}}$ (IC)	0.13
(C) PM versus IC:	
$a_{2\ \text{untreated}}$ (PM) vs. $a_{2\ \text{untreated}}$ (IC)	5.0×10^{-7}
$a_{2\ \text{inhibited}}$ (PM) vs. $a_{2\ \text{inhibited}}$ (IC)	0.042

In Table 5.4 we see that there is a statistical significance between when comparing a variety of values, such as the IC a_1 terms under untreated and inhibited conditions. This is expected since it was shown in Table 5.1 that the rotational times (ϕ) were also statistically different. This same trend is consistent throughout under respective comparisons and conditions. Examining the last two comparisons in Table 5.4 shows that there are significant differences in the membrane and internal compartment a_2 terms for both untreated and STA-200 inhibited conditions (p-value < 0.05). Using this along with the rotational time under untreated conditions, the internal compartment species is much larger than the membrane species. This could be location-dependent dimerization due to the fact that internal compartments have more access to substrate and conditions necessary for acid-base cleavage, as previously stated.[50] An interesting point is that the internal compartment and membrane a_2 under inhibited conditions are also statistically different (p-value < 0.05). This can be explained in the same manner as for untreated

conditions where the IC has access to more substrate which would increase the relative amount of BACE1-EGFP dimerization, resulting in a statistically different hydrodynamic radius. The explanation for the less than 2-fold increase in hydrodynamic radii between species could be a result of segmental motion of the attached EGFP.

5.5 Conclusions

In our studies to test the dimerization hypothesis of BACE1 in cells, we performed 1P-trFA on HEK293 cells expressing the BACE1-EGFP fusion protein under untreated and STA-200 inhibited conditions. Fitting parameters obtained from biexponential decay fitting of anisotropy curves revealed a fast rotating species (<3 ns) that is thought to be due to homoFRET. This is consistent with literature as well as our FLIM results showing a population with lifetimes consistent with homoFRET.[63] By comparing results in untreated HEK293 cells expressing BACE1-EGFP, it is apparent that there are at least two species present. The rotating species with the faster rotational time (ϕ_2 of ~17 ns) that resides on the cell membrane is believed to be the monomeric form of BACE1, while the internal compartment rotating species with the larger value (ϕ_2 of 30-40 ns) is believed to be the dimeric form of BACE1 due to the fact that its rotational time is approximately double that of the membrane species. In addition, as previously hypothesized by the groups of Multhaup and Lendahl, BACE1-EGFP appears to undergo substrate dependent dimerization in both the on the plasma membrane and within an internal compartment.[34,63] To confirm these results, viscosity as well as

STA-200 dose-dependent experiments should be carried out examining the dimerization of BACE1-EGFP in HEK293 cells. Having demonstrated the flexibility of BACE1-EGFP on the nanosecond timescale, the next question that needs to be asked is: based on the translational diffusion and molecular brightness, does BACE1-EGFP act as a dimer or a monomer on the millisecond timescale? To answer this question we utilized fluorescence correlation spectroscopy along with subsequent molecular brightness calculations.

Chapter 6

Translational Diffusion of BACE1-EGFP in the Plasma Membrane of HEK293 Cells Using Fluorescence Fluctuation Analysis

6.1 Summary

The hypothesis herein is that BACE1 forms dimers in cultured HEK cells, which should affect the corresponding translational diffusion as compared with the monomeric counterpart. To test this dimerization hypothesis, we investigate the translational diffusion of genetically encoded BACE1-EGFP in the plasma membrane of adherent cells to quantify both the translational diffusion coefficient and associated molecular brightness using fluorescence correlation spectroscopy (FCS). In these single-molecule studies, the expression level of BACE1-EGFP in transiently transfected HEK293 cells was reduced by a factor of fifty compared to those used for FLIM (Chapter 4) and time-resolved anisotropy (Chapter 5) measurements. These studies were carried out under both untreated and STA-200 inhibited conditions using one-photon (488 nm) FCS. Our rationale stems from the notion that translational movement of a protein like BACE1-EGFP is dependent on its hydrodynamic radius, which is expected to be distinct for monomeric and dimeric species. Under ideal conditions, the molecular brightness (how many fluorescence photons emitted by a molecule crossing the observation volume) of a dimer should be twice that of a monomer. Our 1P fluorescence autocorrelation functions of BACE1-EGFP on the plasma membrane of HEK cells are modeled using two diffusing species on the 2D plasma membrane with estimated diffusion coefficients of 9.0×10^{-7}

cm^2/sec and 3.5 x 10^{-9} cm^2/sec. To differentiate between translational diffusion and laser-induced biophysical processes (such as EGFP blinking), different diffusion models were tested and the corresponding hydrodynamic radii (*a*) were calculated. Our findings are discussed within the context of the dimerization hypothesis, in conjunction with FLIM (Chapter 4) and Anisotropy (Chapter 5) measurements, and relevant literature studies.

6.2 Background

Since its conception in 1972 by Watt W. Webb at Cornell University, fluorescence correlation spectroscopy (FCS) has become the tool of choice for single-molecule studies in both aqueous solutions and biological samples.[46,66] At the single-molecule level, the concentration fluctuations (and therefore the corresponding fluorescence signal) of a fluorophore within an open observation volume are influenced by translational diffusion, photo-physical processes (e.g., triplet state population via intersystem crossing, fluorescence blinking, etc.), and chemical reactions (Eq. 2.5).[47] In FCS, the diffraction-limited observation volume (~10^{-15} L) depends on how tightly the laser beam is focused (i.e., dependent on the numerical aperture (NA) of the microscope objective) as well as the confocal pinhole.[46] The time-dependent fluorescence fluctuation of a single molecule diffusing throughout the observation volume is then autocorrelated as the function of lag time (τ). The corresponding autocorrelation function, $G(\tau)$, depends on the average residency time of the same molecule in the observation volume (see Chapter 2: Materials and Methods). The diffusion time (*D*), and therefore the corresponding diffusion coefficient and hydrodynamic radius, of the diffusing species can

be estimated in 2D (e.g., membrane) and 3D (e.g., cytosol or aqueous solution) in a well-calibrated FCS system.

Using the same FCS approach, the average number of molecules residing in the observation volume (i.e., concentration) and the average fluorescence signal are used together to calculate the molecular brightness (how many fluorescence photons are emitted by a single molecule during its residence time in the observation volume), which depends on the oligomerization state of the molecule (e.g., ideally a relative brightness of 1.0 and 2.0 are expected for monomeric and dimeric states of a molecule, respectively).[67] Previous studies have shown that molecular brightness can be used as a valuable tool to study protein oligomerization.[68-70] For example, Hur *et al.* performed molecular brightness studies on *E. coli* expressing nuclear transport factor 2-EGFP (NTF2-EGFP) using expressed EFGP as a control.[68] Their results indicated that EGFP exists as a monomer while NTF2-EGFP is dimeric.[68] However, brightness applications in cellular and molecular biophysics can be complicated by the difference in the system geometry, laser-induced photobleaching, and competing photophysical processes such as blinking as observed in GFP mutants.[68,71] If not careful, these challenges can undermine the potential of using FCS-measured molecular brightness to quantify the oligomerization state of a protein. To overcome these challenges, fusion protein engineering as well as careful modeling of the observation volume must be employed.

Marquer *et al.* recently reported on the translational diffusion of BACE1-EGFP in HEK293 cells as a means to examine BACE1-EGFP association with membrane lipid rafts as a function of cholesterol concentration.[50] Using one-photon fluorescence

correlation spectroscopy (FCS), the authors observed two diffusing species of BACE1-EGFP on the plasma membrane.[50] The faster diffusing species was assigned to BACE1-EGFP diffusing in a liquid disordered region of the membrane.[50] The second slower diffusing species (80-130 ms diffusion time without explicitly mentioning the corresponding diffusion coefficient, which is independent of experimental setup) of BACE1-EGFP was attributed to the fusion protein partitioned into lipid rafts.[50] This conclusion was based on cholesterol loading of the plasma membrane of HEK cells using a methyl-β-cyclodextrin-cholesterol complex (MβCD).[50] The results showed that cholesterol loading of liquid-ordered regions caused a 60% increase in the diffusion time of the larger BACE1-EGFP species in the raft regions of the plasma membrane. It was not clear, however, how cholesterol depletion might affect the fast diffusing species that was attributed to BACE1-EGFP partitioned into the liquid disordered phase of the plasma membrane.[50] Importantly, the possibility of BACE1-EGFP conformational changes, such as dimerization, was not discussed within the scope of those studies.[50] While EGFP is known to undergo fluorescence blinking in single-molecule studies, it is not clear if or how such blinking was factored into the interpretation of the previous FCS studies of BACE1-EGFP.[50]

In this chapter, we describe 1P-FCS (Chapter 2: Materials and Methods) studies of BACE1-EGFP expressed in transiently transfected adherent HEK cells in culture at room temperature. These studies were carried out under untreated and STA-200 inhibited conditions. Our objective here is to complement our FLIM and time-resolved anisotropy measurements by testing the dimerization hypothesis of BACE1-EGFP using noninvasive

and quantitative approaches. Importantly, such integration will ultimately help to examine the scaling of this dimerization in both space and time domains.

6.3 Materials and Methods

A full description of materials and FCS methods used in this Chapter was described previously (Chapter 2: Materials and Methods). Briefly, HEK293 cells were cultured to ~80% confluency at which point they were sub-cultured and seeded into 35 mm MatTek petri dishes and incubated at 37 °C. After 24 hours the cells were transfected with a Fugene HD^{TM} (a non-liposomal mediated transfection reagent) and BACE1-EGFP vector mixture containing 50-fold less BACE1-EGFP vector than was used for the FLIM and trFA studies (in order to reduce the level of BACE1-EGFP expression), and incubated for 24-48 hours. At least 1 hour prior to measurements, the transfection media was removed and replaced with complete media either with or without the addition of STA-200 inhibitor. FCS measurements were carried out using the system depicted in Figure 2.6 (Chapter 2). Briefly, we first used a wide-field lens in conjunction with a 488 nm laser on an Olympus microscope to locate fluorescent cells and obtain the desired x- and y-coordinates. Next, we switched to the FCS setup and identified the corresponding z-coordinate using the 488 nm laser to excite the sample. The time-dependent epi-fluorescence fluctuation was detected, autocorrelated, stored, and analyzed.

6.4 Results and Discussion

6.4.1 Calibration of our FCS Setup using Rhodamine Green and EGFP in a Buffer

Careful alignment and calibration of our home-built FCS was carried out using Rhodamine Green (RhG, 60 nM) in an aqueous droplet (PBS, pH 7.6) on a microscopy coverslip at room temperature. The fluorescence fluctuation autocorrelation of RhG was recorded using 488-nm excitation via a 1.2NA, water immersion objective (see Chapter 2: Materials and Methods). An optical fiber with a 50-μm diameter served as a confocal pinhole. A representative RhG fluorescence fluctuation autocorrelation function is shown in Figure 6.1 (curve 1), which is best described by fluctuation due to diffusion and an exponential term to account for the formation of a triplet state population under our laser conditions (Equation 2.6). The estimated diffusion time of RhG in our laser and optics induced observation volume is 0.124 ± 0.003 ms. The reported diffusion coefficient for Rhodamine derivatives is 2.8×10^{-6} cm^2/s in a buffer at room temperature.[41] Based on the relationship between the diffusion time (τ) and diffusion coefficient (D) (Equation 2.9), the volume and the lateral extension (ω_{xy}) of our observation volume are roughly 8.8×10^{-16} L and 370 nm, respectively. The autocorrelation function of free EGFP (in PBS, pH 7.8) was measured under the same conditions (Figure 6.1, Curve 2) using the same FCS setup with an estimated diffusion coefficient of 2.6×10^{-7} cm^2/s. This calibration using RhG was repeated twice every day during the course of these experiments.

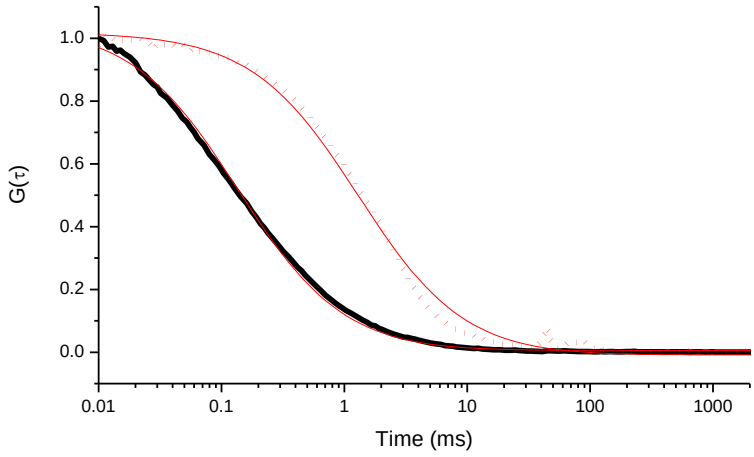

Figure 6.1: Representative Autocorrelation Curve of HEK293 Cells Expressing BACE1-EGFP. Representative fitted lines (solid red) for Rhodamine Green in buffer (solid), EGFP in buffer (dotted).

Fluorescence fluctuation autocorrelation of BACE1-EGFP in cultured, adherent HEK cells were carried out under the same conditions. Once the FCS system was calibrated, the same experimental conditions were maintained during the whole set of measurements on live HEK cells expressing BACE1-EGFP. The only exception in experimental conditions was the excitation laser intensity, which was varied based on the expression level to ensure a good signal-to-noise ratio for the measured anisotropy decays. The laser beam was focused on multiple random locations on the plasma membrane of the cultured HEK cells expressing BACE1-EGFP (Figure 6.2) to ensure representative sampling of the system.

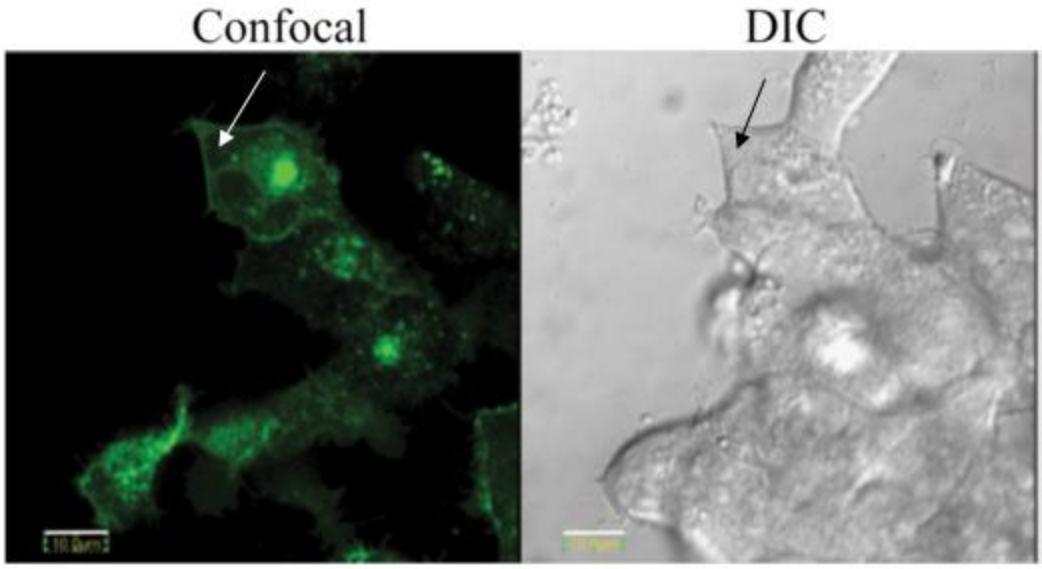

Figure 6.2: Cellular Locations of FCS Measurements. Confocal (left), DIC (right), arrows point to representative locations of FCS measurements on plasma membrane.

6.4.2 Fluorescence Fluctuation Autocorrelation of BACE1-EGFP Expressed in the Plasma Membrane of HEK Cells

BACE1 is hypothesized to form a dimer; however, this has not yet been demonstrated in cells. To test this hypothesis, we investigated the translational movement and molecular brightness of BACE1-EGFP transiently expressed in HEK293 cells under untreated and STA-200 inhibited conditions. Representative fluorescence fluctuation autocorrelation curves of BACE1-EGFP are shown in Figure 6.3 under untreated and STA-200 inhibited conditions. As a control, the 3D autocorrelation function of RhG recorded under the same conditions is shown for visual comparison (Figure 6.2, solid black line).

It is worth mentioning that even at the lowest expression level of BACE1-EGFP in HEK cells, the number of molecules was too high to yield an autocorrelation curve

without photobleaching. This is consistent with the notion that the zero-time amplitude of the correlation function is inversely proportional to the number of molecules residing in the observation volume. As the number of molecules increases, the amplitude of the correlation function decreases. Once photobleaching was complete, the fluorescence fluctuation of the remaining BACE1-EGFP molecules on the plasma membrane was autocorrelated with non-zero amplitude. It should be noted that the observed autocorrelation functions used in these studies here were reported only once the photobleaching was complete.

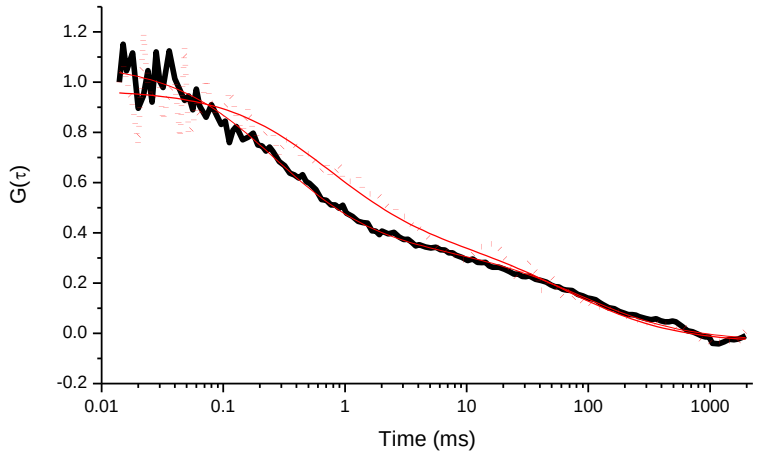

Figure 6.3: Representative Autocorrelation Curve of HEK293 Cells Expressing BACE1-EGFP. Untreated (solid black) and STA-200 inhibited (dotted) with the corresponding best fit lines (solid red).

The autocorrelation function, *G(τ)*, for BACE1-EGFP was analyzed using a two-diffusing species model (Untreated conditions: N = 21, STA-200 Inhibited conditions: N

= 46) in two-dimensions (2D) as described in Equation 2.8 (chapter 2). The fluorescence autocorrelation fitting parameters for BACE1-EGFP under untreated and inhibited conditions are summarized in Table 6.1. To examine whether the autocorrelation function and fitting parameters of untreated and inhibited BACE1-EGFP were statistically significant, we calculated the corresponding *p*-values using Welsh's *t*-test (Table 6.1).

Table 6.1: Fluorescence Autocorrelation Fitting Parameters for a Two-Diffusing BACE1-EGFP Species in Two-Dimensions Model (*p*-values were obtained using Welsh's *t*-test)

Fitting Parameters	Untreated (N = 21)	Inhibited (N = 43)	*p*-value
N	11.0 ± 6.8	20 ± 14	N/A[a]
τ_1 (ms, N = 44)	0.40 ± 0.31	0.40 ± 0.22	0.90
τ_2 (ms, N = 42)	121 ± 155	80 ± 85	0.25
f	0.50 ± 0.13	0.50 ± 0.15	0.25
Photon Count	20 ± 14	20 ± 19	0.95

[a] *N is dependent on the expression level of BACE1-EGFP at the site of measurement.*

From Table 6.1 it is clear that there is substantial variation among the different trials as manifest by standard deviations present that occasionally exceed the mean value. This could be due to the complexity of the cellular environment, in which case the number of measurements needed to ascertain accurate diffusion times would be quite substantial (>80 trials). Due to this wide range of values and based on our Welsh's *t*--test, we conclude that there is no statistical difference in the fitting parameters of BACE1-EGFP autocorrelations under untreated and STA-200 inhibited conditions in HEK cells.

Even under STA-200 inhibited conditions, it is conceivable that the observed wide range of the slow diffusion time (τ_2) can be attributed to different populations of monomeric and dimeric BACE1-EGFP in the plasma membrane.

6.4.3 Diffusion Coefficient and Hydrodynamic Radius Calculations of BACE1-EGFP Expressed in the Plasma Membrane of HEK Cells

The fitting parameters are summarized in Table 6.1 and were used to calculate the corresponding diffusion coefficients (D), hydrodynamic radii (a), and molecular brightness for BACE1-EGFP expressed in HEK293 cells (Table 6.2).

Table 6.2: BACE1-EGFP Average Diffusion, Hydrodynamic Radii and Molecular Brightness from FCS (Control EGFP Brightness: Untreated = 2.6, Inhibited = 10.3) Hydrodynamic radii calculated using the Stokes-Einstein model (Eq. 2.10) with membrane-like viscosity = 4.5 cP, T = 295 K, and $k_B = 1.38 \times 10^{-16}$ g*cm^2/s^2*K

	D_1 (cm^2/sec)	D_2 (cm^2/sec)
Untreated (N=21)	$9.0 \times 10^{-7} \pm 6.9 \times 10^{-7}$	$3.0 \times 10^{-9} \pm 3.7 \times 10^{-9}$
Inhibited (N = 42-44)	$9.0 \times 10^{-7} \pm 4.9 \times 10^{-7}$	$4.0 \times 10^{-9} \pm 4.7 \times 10^{-9}$
p-value (t-test)	0.93	0.77

	a_1 (nm)	a_2 (nm)	Brightness
Untreated (N=21)	0.50 ± 0.69	159 ± 128	2.0 ± 2.4
Inhibited (N = 42-44)	0.50 ± 0.98	119 ± 102	1.0 ± 1.65
p-value (t-test)	0.78	0.16	0.74

The first, apparent diffusion coefficient (D_1) is significantly faster, $(9.0 \pm 6.9) \times 10^{-7}$ cm^2/sec, than what is expected for a fusion protein the size of BACE1-EGFP (75 + 29 kDa) when considering that free EGFP in mammalian cytoplasm has a diffusion

coefficient of 5.1 x 10^{-7} cm^2/sec.[65] It is possible that the fast component in the BACE1-EGFP autocorrelation in the plasma membrane is due to EGFP blinking, which would agree with previous biophysical studies on MHC-class I protein genetically encoded with EGFP in a range of environments.[72] In addition to the translational diffusion component, the authors observed a fast decay component of MHCI-EGFP autocorrelation. To examine whether this fast component (τ_1 = 0.5 ms, D_1 = 9.0 x 10^{-7} cm^2/s) was due to GFP blinking or a fast diffusing species, FCS experiments were carried out as a function of the confocal pinhole size. As predicted, the slow diffusion time increased when a larger confocal pinhole was used. In contrast, the reported fast component was independent of the fiber diameter (i.e., confocal pinhole) and was attributed to EGFP blinking.[72] The observed fast autocorrelation component of BACE1-EGFP seems to agree with recent studies on EGFP-tagged MHC (I) protein.[72]

In addition, the observed second diffusion coefficient (D_2) of BACE1-EGFP (4.0 x 10^{-9} ± 4.7 x 10^{-9} cm^2/sec) in the plasma membrane seems comparatively slow compared to previous studies on the trimeric glutamate transporter in model membranes (4 x 10^{-8} cm^2/s).[73] Such a difference can be attributed to the complexity associated with the plasma membrane of living cells compared to the lipid bilayer in model membranes. It is also possible that our measurements sample different oligomeric states of BACE1-EGFP in regions of the plasma membrane with diverse biophysical properties such as liquid ordered and disordered regions.

6.4.4 Model-Based Calculations of the Diffusion Coefficient of BACE1-EGFP Expressed in the Plasma Membrane of HEK Cells

Table 6.3: Hydrodynamic Radii of BACE1-EGFP calculated using Saffman-Delbrück Equation for Membrane Protein Diffusion.

R_{SD}	a_2 (nm)
Untreated	>200
Inhibited	>200

This inconsistency between observed and expected values is propagated even further with the calculated hydrodynamic radii. The second species has radius of approximately 119 nm, which is very different from the expected hydrodynamic radius for a 100 kDa protein (~4 nm).[74] Using Saffman-Delbrück model (Chapter 2), we made the following assumptions: membrane height = 5 nm, viscosity of medium = 2 cP, viscosity of the membrane = 100 cP and T = 295 K (all consistent with literature).[41,75] In the Saffman-Delbrück model for the translational diffusion of a transmembrane protein, it is assumed that different moieties will be exposed to different environmental constraints. Here we assumed that the viscosity of the plasma membrane (100 cP), the cytosol (6 cP) and the culture media as water at room temperature (2 cP).[75,76] Based on literature studies, we also assumed that the hydrodynamic radius of BACE1-EGFP (molecular weight = ~105 kDa) is ~4.2 nm.[74] Using this model, we estimated a diffusion coefficient of 2.27 x 10^{-8} cm^2/s on the plasma membrane under untreated conditions.

The fast component yields a hydrodynamic radius that is so small that the model breaks down, which is unexpected for genetically encoded fusion proteins. Alternatively,

the fast decay component is likely to be attributed to the well-documented fluorescence blinking of EGFP first described by Dickson *et al.* using single-molecule studies of green fluorescence proteins immobilized on a glass substrate (1 s blinking time).[71,77] Using FCS on free EGFP and other mutants in buffers at room temperature, Webb and coworkers reported a blinking times of 0.045 ms, some of which were pH and laser-intensity dependent.[71,77] The pH-blinking was attributed to EGFP protonation for a fraction constituting 80% of the protein population.[71] The fast autocorrelation time observed here for BACE1-EGFP is consistent with the timescale of the reported blinking of GFP mutants. The enhanced amplitude fraction of the blinking population, however, is likely due to the laser intensity as well as the restriction imposed on BACE1-EGFP by the plasma membrane. Such a restriction on the fusion protein mobility enhances the fraction of blinking due to the fact that the construct spends longer time in the observation volume. As a result, we conclude that the fast decay time of the autocorrelation function of BACE1-EGFP expressed in the plasma membrane of HEK cells is more likely to be due to EGFP blinking rather than to the nature of the lipid domains (liquid disordered or fluidic domain) as reported by Marquer and co-workers.[50] The possibility of triplet state contribution to the observed fast decay component of the autocorrelation function can be ruled out for BACE1-EGFP based on the expected fast timescale of triplet state lifetime (tens of microseconds).[78] As for the slow diffusion time (121 ± 155 ms) and corresponding diffusion coefficient ($4.0 \times 10^{-9} \pm 4.7 \times 10^{-9}$ cm^2/sec) can be understood in terms of the hydrodynamic radius of BACE1-EGFP, membrane restriction, and the possibility of populations of monomeric and dimeric fusion proteins.

Since our data shows signs of EGFP blinking, it is reasonable to infer that molecular brightness calculations may be compromised by bleaching and may no longer be a valid approach to test oligomerization of BACE1-EGFP. This is apparent in Table 6.2. The molecular brightness values vary greatly due to large standard deviations and a *t*-test *p*-value >0.05, consistent with other measurements throughout our FCS experiments. In addition, molecular brightness values differ greatly from the EGFP in a buffer control, indicating that we may need to consider a new control for the BACE1-EGFP monomer. Such a control should take into account the orientation and membrane bound properties of BACE1-EGFP. One such possibility would be designing an EGFP with a membrane anchor that would be expressed throughout the cell. This would provide a membrane-bound monomeric fluorescent species with similar orientation to BACE1-EGFP. Also, due to the presence of blinking it is advisable that parameters pertaining to expression and laser intensity in future FCS studies should be optimized to reduce blinking. If blinking cannot be avoided, experiments should be carried out using blinking assisted localization microscopy. In these experiments blinking is utilized to observe the absence of fluorescent fluctuation to track fluorophores.[79] An alternative method would be to use a model that accounts for blinking when fitting autocorrelation curves.[80]

By comparing the measured (4.0×10^{-9} cm^2/s) and calculated (2.27×10^{-8} cm^2/s) diffusion coefficients for the slow diffusing species, it is clear that the measured value is approximately 20-fold slower than the theoretical diffusion coefficient, which cannot be accounted for even with different viscosity values.[74] The observed slow diffusing species in our FCS experiment is likely to be immobilized in our anisotropy measurements on the

nanosecond timescale. Using the Saffman-Delbruck model to calculate translational properties of transmembrane proteins, the calculated hydrodynamic radii are not reasonable for protein diffusion inside a membrane and the model fails to accurately describe the measured processes. Due to large standard deviations in the slow diffusing species and mean values that differ from previous BACE1-EGFP translational diffusion experiments done by Marquer *et al.*, no deductions can be made regarding the monomeric or dimeric state of BACE1-EGFP based on FCS results.[50] Although it is important to note that in the absence of blinking, BACE1-EGFP seems to exist as a single diffusing species that should be modeled by 2-dimensional anomalous diffusion.

6.5 Conclusions

To test the dimerization hypothesis of BACE1, we used one-photon fluorescence correlation spectroscopy to measure the translational movement and brightness of BACE1-EGFP expressed in HEK293 cells under untreated and STA-200 inhibited conditions. Two apparent diffusion times were observed within estimated diffusion coefficients, (9.0×10^{-7} cm^2/sec and 3.5×10^{-9} for species τ_1 and τ_2, respectively). These measured values are significantly different from what we calculated using the Saffman-Delbrück model (diffusion coefficient = 2.27×10^{-8} cm^2/s) for BACE1-EGFP expressed in HEK293 cells. This difference is even larger when using the Saffman-Delbrück model with an estimated hydrodynamic radii much larger (>200 nm) than expected (4.2 nm).[74] The large standard deviation in τ_2 may suggest a diverse population of BACE1-EGFP with distinct oligomerization states and local heterogeneity in membrane domains (rafts).

In addition, the fast diffusion time is assigned as laser-induced blinking of EGFP in our fusion protein. Additional fitting models are currently being considered for fitting autocorrelation curves such as blinking assisted localization microscopy which utilizes blinking to study translational diffusion.[79,80]

Chapter 7

Conclusions and Future Directions

7.1 Overall Conclusions

Previously, detergent-based extraction studies had been utilized to provide evidence that suggest BACE1 forms dimers as a function of substrate binding.[34,35,81] To test the dimerization hypothesis of BACE1 in intact, living cells, we used integrated, non-invasive fluorescence micro-spectroscopic techniques to study the BACE1-EGFP fusion protein expressed in adherent HEK293 cell as model system. These studies were carried out on multiple timescales and at multiple molecular sensitivities to probe different molecular processes of BACE1-EGFP transfected HEK cells under untreated and STA-200 inhibited conditions. The rationale is that STA-200 would induce BACE1 dimerization as compared with the resting, non-treated cells. As proposed previously, BACE1 utilizes active site recognition of substrate to induce dimerization. [34,36] This concept was demonstrated using active site mutagenesis in tandem with detergent-based dimerization studies.[36]

Our confocal and DIC microscopy results confirm that transiently transfected HEK293 cells express BACE1-EGFP both at the plasma membrane and within the cell interior. Based on our current understanding of BACE1, the BACE1-EGFP is expressed in Golgi apparatus. The BACE1-EGFP expressing HEK293 cells remained viable with no observed adverse effects as shown by the cell morphology over the time courses of the

outlined experiments. Z-stacked confocal imaging of transfected cells provided three-dimensional images of BACE1-EGFP throughout the adherent cells (data not shown). The confocal and DIC imaging microscopy was carried out during the course of two-photon FLIM measurements to ensure cell viability and negligible laser-induced photostress and photodamage, especially for two-photon fluorescence microscopy. These confocal images also allowed us to examine the distribution of BACE1-EGFP near the cell surface-glass interface, through a cell cross-section, and near the top plasma membrane of the adherent HEK cells.

Two-photon FLIM imaging was used to examine any changes in the conformation and surrounding local environment of BACE1-EGFP in cultured HEK cells. Our frequency-weighted pixel analysis (fluorescence lifetime histograms) of these FLIM images indicated the existence of two BACE1-EGFP subpopulations with distinct fluorescence lifetimes (2.4 and 2.1 ns). The subpopulation of BACE1-EGFP with the shorter fluorescence lifetime was assigned to BACE1-EGFP dimers undergoing homo-FRET. In contrast, the subpopulation with the longer fluorescence lifetime was assigned to a monomeric BACE1-EGFP population. Double Gaussian fits of the histograms for each FLIM image were used to assess the energy transfer efficiency and intermolecular distance between the two BACE1-EGFP in the dimer. When cells were incubated with the STA-200 transition state analog inhibitor, a trend emerged for FLIM images recorded near the cell surface-glass interface, with a shift to the subpopulation corresponding to the shorter fluorescence lifetime (i.e., undergoing homo-FRET). Analysis of areas under fitted Gaussian curves revealed no statistical difference (p-value > 0.05) between

untreated and STA-200 inhibited conditions. This is most likely do to small sample size (n=5). Another possibility is that STA-200 inhibition of BACE1-EGFP is a time-dependent process. Our FLIM-based homo-FRET suggests an efficiency of 11% under the expression level used in these studies. In addition, we estimated an intermolecular distance between the BACE1-EGFP molecules in the dimer to be 6.5 nm.

To test the structural flexibility and the dimerization hypothesis of BACE1-EGFP in HEK cells, we conducted time-resolved anisotropy measurements for real-time monitoring of the rotation (or tumbling) motion on the picosecond to nanosecond timescale. It is important to mention that on this fast time scale, translational diffusion is too slow and the existing populations of BACE1-EGFP are basically frozen in time as we record our fast molecular snapshots. Subsequent fitting of anisotropy curves required a biexponential decay model to accurately represent the data. The first rotational time (ϕ_1) was found to be 0.4-2.3 ns, which is much shorter than the rotational mobility of free EGFP in pure buffer or in living cells (~10 ns).[56] As a result, such fast rotational component was attributed to homo-FRET, which is also consistent with previous studies involving dimerization of the amyloid precursor protein.[63] The second rotational time (ϕ_2) was much longer (between 17 and 40 ns) but displayed characteristics of segmental motion of the EGFP moiety due to the fact that the overall BACE1-EGFP (~105 kDa) was restricted by the plasma membrane (in a buffer BACE1-EGFP would have a rotational time of ~110 ns) although it can be noted that the accuracy of the anisotropy measurements decreases as the rotational time increases by orders of magnitudes relative to the corresponding excited-state lifetime.[63] However, we believe that our excellent

signal-to-noise ratio and the estimated slow rotational time is significantly faster than an estimated 80 ns rotational time for a protein of this size.[63] The slow rotational time depends on the cellular compartmentalization of BACE1-EGFP as well as the environmental conditions of the HEK cells (untreated versus inhibited). For example, we found that the rotation of BACE1-EGFP on the plasma membrane under untreated and inhibited conditions was statistically different (p-value < 0.05) as a monomer under untreated conditions (~17 ns) than as a dimer under STA-200 inhibited conditions (~28 ns). With rotational times for substrate-induced dimerization being consistent with rotational times for BACE1-EGFP in the Golgi apparatus, we deduce that internal species also exist as a dimer.

To compare the temporal scaling and the molecular averaging inherent in FLIM and anisotropy measurements, we utilized FCS to measure the translational diffusion of BACE1-EGFP on the millisecond timescale, where the diffusion coefficient is inversely proportional to the hydrodynamic radius of the diffusing molecule. Autocorrelation curves revealed the existence of two diffusing species with an estimated translational diffusion coefficients of 9.0×10^{-7} and 3.5×10^{-9} cm^2/sec for species τ_1 and τ_2, respectively. We believe that the fast component is due to EGFP blinking. The slow component is assigned to BACE1-EGFP, but due to the complex cellular environment and possibility of different oligomeric states of BACE1-EGFP, the resulting standard deviations are too large to draw any conclusions as to whether or not BACE1-EGFP exists as a monomer or dimer based on FCS data.

By comparing results from both 2P-FLIM and 1P-trFA, it is evident that BACE1-EGFP undergoes homoFRET to varying degrees, which would be expected in its dimeric form. In addition, the 1P-trFA data suggest that this homoFRET is accompanied by what appears to be STA-200 induced dimerization due to an approximate doubling of rotational time seen at the cell surface-glass coverslip interface. Comparisons of rotational times of induced dimerization at the membrane and internal compartments such as the Golgi apparatus lead us to believe that BACE1-EGFP also exists as a dimer intracellularly, possibly due to its close proximity to endogenous substrates such as APP.

Our results indicate a likely dimerization of BACE1-EGFP, which may play an important role in its biological function and association with substrates such as APP. However, further study of this process is important in understanding the biochemistry and molecular biology of BACE1 and its involvement in Alzheimer's disease.

7.2 Future Directions

The results reported here open the door for related projects to further elucidate the structure-function relationship of BACE1 in its natural environment in living cells or tissues. To confirm that BACE1-EGFP is indeed localized to the Golgi apparatus, for example, we are planning to carry out co-localization studies between BACE1-EGFP and Golgi apparatus specific markers. In addition, we are planning to mutate both active site aspartate residues which could serve as a possible positive control for BACE1-EGFP dimerization based on the reported studies by Lendahl and co-workers.[36] For FCS,

BACE1-EGFP expression and laser intensity need to be optimized further to reduce the contribution of EGFP photobleaching and perhaps blinking. Alternatively, fluorescence techniques such as BaLM can utilize the blinking characteristic of EGFP to track translational diffusion.

We are also planning to use fluorescence cross-correlation spectroscopy on transiently transfected HEK cells co-expressing both BACE1-EGFP fusion protein as well as fluorescently labeled substrate (e.g., APP) to investigate BACE1-substrate binding and its resulting dimerization. For future FLIM experiments, sample sizes should be much larger to improve the statistical analyses of the results.

To further explore the effects of STA-200 on substrate-induced dimerization, all fluorescence techniques with STA-200 should be conducted in a dose-dependent manner. Since the accumulation of amyloid beta fragments is a hallmark of Alzheimer's disease, we will investigate the effects of protein crowding inherent in living cells and tissues on BACE1-EGFP dimerization. These studies will parallel ongoing experiments aimed at elucidating the macromolecular crowding effects on diffusion, biochemical reaction kinetics, and protein folding under controlled conditions. Finally, these recommended BACE1-EGFP dimerization studies could be expanded to include other BACE1 isoforms in potentially more relevant neural cell lines.

References

(1) Association, A. s.; Alzheimer's Association: 2015; Vol. 2015.

(2) Vassar, R.; Kuhn, P. H.; Haass, C.; Kennedy, M. E.; Rajendran, L.; Wong, P. C.; Lichtenthaler, S. F. *J Neurochem* **2014**, *130*, 4.

(3) van der Kant, R.; Goldstein, L. S. *Dev Cell* **2015**, *32*, 502.

(4) Kang, J.; Lemaire, H. G.; Unterbeck, A.; Salbaum, J. M.; Masters, C. L.; Grzeschik, K. H.; Multhaup, G.; Beyreuther, K.; Muller-Hill, B. *Nature* **1987**, *325*, 733.

(5) Citron, M.; Teplow, D. B.; Selkoe, D. J. *Neuron* **1995**, *14*, 661.

(6) Seubert, P.; Oltersdorf, T.; Lee, M. G.; Barbour, R.; Blomquist, C.; Davis, D. L.; Bryant, K.; Fritz, L. C.; Galasko, D.; Thal, L. J.; et al. *Nature* **1993**, *361*, 260.

(7) Haass, C.; Selkoe, D. J. *Cell* **1993**, *75*, 1039.

(8) De Strooper, B. *Neuron* **2003**, *38*, 9.

(9) Glenner, G. G.; Wong, C. W. *Biochemical and Biophysical Research Communications* **1984**, *120*, 885.

(10) Masters, C. L.; Simms, G.; Weinman, N. A.; Multhaup, G.; McDonald, B. L.; Beyreuther, K. *Proc Natl Acad Sci U S A* **1985**, *82*, 4245.

(11) Goedert, M.; Wischik, C. M.; Crowther, R. A.; Walker, J. E.; Klug, A. *Proc Natl Acad Sci U S A* **1988**, *85*, 4051.

(12) Buee, L.; Bussiere, T.; Buee-Scherrer, V.; Delacourte, A.; Hof, P. R. *Brain Res Brain Res Rev* **2000**, *33*, 95.

(13) Itagaki, S.; McGeer, P. L.; Akiyama, H.; Zhu, S.; Selkoe, D. *J Neuroimmunol* **1989**, *24*, 173.

(14) Van Broeck, B.; Vanhoutte, G.; Pirici, D.; Van Dam, D.; Wils, H.; Cuijt, I.; Vennekens, K.; Zabielski, M.; Michalik, A.; Theuns, J.; De Deyn, P. P.; Van der Linden, A.; Van Broeckhoven, C.; Kumar-Singh, S. *Neurobiol Aging* **2008**, *29*, 241.

(15) Sisodia, S. S.; Koo, E. H.; Beyreuther, K.; Unterbeck, A.; Price, D. L. *Science* **1990**, *248*, 492.

(16) Haass, C.; Hung, A. Y.; Schlossmacher, M. G.; Teplow, D. B.; Selkoe, D. J. *J Biol Chem* **1993**, *268*, 3021.

(17) Vassar, R. *J Mol Neurosci* **2001**, *17*, 157.

(18) Yan, R.; Bienkowski, M. J.; Shuck, M. E.; Miao, H.; Tory, M. C.; Pauley, A. M.; Brashier, J. R.; Stratman, N. C.; Mathews, W. R.; Buhl, A. E.; Carter, D. B.; Tomasselli, A. G.; Parodi, L. A.; Heinrikson, R. L.; Gurney, M. E. *Nature* **1999**, *402*, 533.

(19) Sinha, S.; Anderson, J. P.; Barbour, R.; Basi, G. S.; Caccavello, R.; Davis, D.; Doan, M.; Dovey, H. F.; Frigon, N.; Hong, J.; Jacobson-Croak, K.; Jewett, N.; Keim, P.; Knops, J.; Lieberburg, I.; Power, M.; Tan, H.; Tatsuno, G.; Tung, J.; Schenk, D.; Seubert, P.; Suomensaari, S. M.; Wang, S.; Walker, D.; Zhao, J.; McConlogue, L.; John, V. *Nature* **1999**, *402*, 537.

(20) Hussain, I.; Powell, D.; Howlett, D. R.; Tew, D. G.; Meek, T. D.; Chapman, C.; Gloger, I. S.; Murphy, K. E.; Southan, C. D.; Ryan, D. M.; Smith, T. S.; Simmons, D. L.; Walsh, F. S.; Dingwall, C.; Christie, G. *Mol Cell Neurosci* **1999**, *14*, 419.

(21) Lin, X.; Koelsch, G.; Wu, S.; Downs, D.; Dashti, A.; Tang, J. *Proc Natl Acad Sci U S A* **2000**, *97*, 1456.

(22) Vassar, R.; Bennett, B. D.; Babu-Khan, S.; Kahn, S.; Mendiaz, E. A.; Denis, P.; Teplow, D. B.; Ross, S.; Amarante, P.; Loeloff, R.; Luo, Y.; Fisher, S.; Fuller, J.; Edenson, S.; Lile, J.; Jarosinski, M. A.; Biere, A. L.; Curran, E.; Burgess, T.; Louis, J. C.; Collins, F.; Treanor, J.; Rogers, G.; Citron, M. *Science* **1999**, *286*, 735.

(23) Haniu, M.; Denis, P.; Young, Y.; Mendiaz, E. A.; Fuller, J.; Hui, J. O.; Bennett, B. D.; Kahn, S.; Ross, S.; Burgess, T.; Katta, V.; Rogers, G.; Vassar, R.; Citron, M. *J Biol Chem* **2000**, *275*, 21099.

(24) Costantini, C.; Ko, M. H.; Jonas, M. C.; Puglielli, L. *Biochem J* **2007**, *407*, 383.

(25) Benjannet, S.; Elagoz, A.; Wickham, L.; Mamarbachi, M.; Munzer, J. S.; Basak, A.; Lazure, C.; Cromlish, J. A.; Sisodia, S.; Checler, F.; Chretien, M.; Seidah, N. G. *J Biol Chem* **2001**, *276*, 10879.

(26) Vetrivel, K. S.; Meckler, X.; Chen, Y.; Nguyen, P. D.; Seidah, N. G.; Vassar, R.; Wong, P. C.; Fukata, M.; Kounnas, M. Z.; Thinakaran, G. *J Biol Chem* **2009**, *284*, 3793.

(27) Pastorino, L.; Ikin, A. F.; Nairn, A. C.; Pursnani, A.; Buxbaum, J. D. *Mol Cell Neurosci* **2002**, *19*, 175.

(28) Sannerud, R.; Declerck, I.; Peric, A.; Raemaekers, T.; Menendez, G.; Zhou, L.; Veerle, B.; Coen, K.; Munck, S.; De Strooper, B.; Schiavo, G.; Annaert, W. *Proc Natl Acad Sci U S A* **2011**, *108*, E559.

(29) von Arnim, C. A.; Tangredi, M. M.; Peltan, I. D.; Lee, B. M.; Irizarry, M. C.; Kinoshita, A.; Hyman, B. T. *J Cell Sci* **2004**, *117*, 5437.

(30) He, W.; Lu, Y.; Qahwash, I.; Hu, X. Y.; Chang, A.; Yan, R. *Nat Med* **2004**, *10*, 959.

(31) Hong, L.; Koelsch, G.; Lin, X.; Wu, S.; Terzyan, S.; Ghosh, A. K.; Zhang, X. C.; Tang, J. *Science* **2000**, *290*, 150.

(32) Turner, R. T., 3rd; Hong, L.; Koelsch, G.; Ghosh, A. K.; Tang, J. *Biochemistry* **2005**, *44*, 105.

(33) Munter, L. M.; Sieg, H.; Bethge, T.; Liebsch, F.; Bierkandt, F. S.; Schleeger, M.; Bittner, H. J.; Heberle, J.; Jakubowski, N.; Hildebrand, P. W.; Multhaup, G. *J Am Chem Soc* **2013**, *135*, 19354.

(34) Schmechel, A.; Strauss, M.; Schlicksupp, A.; Pipkorn, R.; Haass, C.; Bayer, T. A.; Multhaup, G. *J Biol Chem* **2004**, *279*, 39710.

(35) Westmeyer, G. G.; Willem, M.; Lichtenthaler, S. F.; Lurman, G.; Multhaup, G.; Assfalg-Machleidt, I.; Reiss, K.; Saftig, P.; Haass, C. *J Biol Chem* **2004**, *279*, 53205.

(36) Jin, S.; Agerman, K.; Kolmodin, K.; Gustafsson, E.; Dahlqvist, C.; Jureus, A.; Liu, G.; Falting, J.; Berg, S.; Lundkvist, J.; Lendahl, U. *Biochem Biophys Res Commun* **2010**, *393*, 21.

(37) Yu, Q.; Proia, M.; Heikal, A. A. *J Biomed Opt* **2008**, *13*, 041315.

(38) Stephens, D. J.; Allan, V. J. *Science* **2003**, *300*, 82.

(39) Becker, W.; Bergmann, A.; Hink, M. A.; Konig, K.; Benndorf, K.; Biskup, C. *Microsc Res Tech* **2004**, *63*, 58.

(40) Zhao, Q.; Young, I. T.; de Jong, J. G. *J Biomed Opt* **2011**, *16*, 086007.

(41) Ariola, F. S.; Li, Z.; Cornejo, C.; Bittman, R.; Heikal, A. A. *Biophys J* **2009**, *96*, 2696.

(42) Jakobs, S.; Subramaniam, V.; Schonle, A.; Jovin, T. M.; Hell, S. W. *FEBS Lett* **2000**, *479*, 131.

(43) Lakowicz, J. R. *Principles of Fluorescence Spectroscopy*; 2nd ed.; Kluwer Academic: New York, 1999.

(44) Kubin, R. F.; Fletcher, A. N. *Journal of Luminescence* **1982**, *27*, 455.

(45) Saha, R.; Verma, P. K.; Rakshit, S.; Saha, S.; Mayor, S.; Pal, S. K. *Sci Rep* **2013**, *3*, 1580.

(46) Hess, S. T.; Huang, S.; Heikal, A. A.; Webb, W. W. *Biochemistry* **2002**, *41*, 697.

(47) Schwille, P.; Haupts, U.; Maiti, S.; Webb, W. W. *Biophys J* **1999**, *77*, 2251.

(48) Hess, S. T.; Sheets, E. D.; Wagenknecht-Wiesner, A.; Heikal, A. A. *Biophys J* **2003**, *85*, 2566.

(49) Stepanenko, A. A.; Dmitrenko, V. V. *Gene* **2015**, *569*, 182.

(50) Marquer, C.; Devauges, V.; Cossec, J. C.; Liot, G.; Lecart, S.; Saudou, F.; Duyckaerts, C.; Leveque-Fort, S.; Potier, M. C. *FASEB J* **2011**, *25*, 1295.

(51) Yamada, T.; Sasaki, H.; Dohura, K.; Goto, I.; Sakaki, Y. *Biochem Biophys Res Commun* **1989**, *158*, 906.

(52) Yellen, G.; Mongeon, R. *Curr Opin Chem Biol* **2015**, *27*, 24.

(53) von Arnim, C. A.; Kinoshita, A.; Peltan, I. D.; Tangredi, M. M.; Herl, L.; Lee, B. M.; Spoelgen, R.; Hshieh, T. T.; Ranganathan, S.; Battey, F. D.; Liu, C. X.; Bacskai, B. J.; Sever, S.; Irizarry, M. C.; Strickland, D. K.; Hyman, B. T. *J Biol Chem* **2005**, *280*, 17777.

(54) Wang, W.; Liu, Q.; Zhan, C.; Barhoumi, A.; Yang, T.; Wylie, R. G.; Armstrong, P. A.; Kohane, D. S. *Nano Lett* **2015**.

(55) Sun, Y.; Wallrabe, H.; Seo, S. A.; Periasamy, A. *Chemphyschem* **2011**, *12*, 462.

(56) Hink, M. A.; Griep, R. A.; Borst, J. W.; van Hoek, A.; Eppink, M. H.; Schots, A.; Visser, A. J. *J Biol Chem* **2000**, *275*, 17556.

(57) Suhling, K.; Siegel, J.; Phillips, D.; French, P. M.; Leveque-Fort, S.; Webb, S. E.; Davis, D. M. *Biophys J* **2002**, *83*, 3589.

(58) van Manen, H. J.; Verkuijlen, P.; Wittendorp, P.; Subramaniam, V.; van den Berg, T. K.; Roos, D.; Otto, C. *Biophys J* **2008**, *94*, L67.

(59) Nalivaeva, N. N.; Turner, A. J. *FEBS Lett* **2013**, *587*, 2046.

(60) Yantsevich, A. V., ; Harnostai, I. N,; Lukashevich,O. P,; Gilep, A. A,; Usanov, S. A. *Biochemistry (Moscow)* **2006**, *72*, 77.

(61) Tramier, M.; Coppey-Moisan, M. *Methods Cell Biol* **2008**, *85*, 395.

(62) Chan, F. T.; Kaminski, C. F.; Kaminski Schierle, G. S. *Chemphyschem* **2011**, *12*, 500.

(63) Devauges, V.; Marquer, C.; Lecart, S.; Cossec, J. C.; Potier, M. C.; Fort, E.; Suhling, K.; Leveque-Fort, S. *PLoS One* **2012**, *7*, e44434.

(64) Heikal, A. A.; Hess, S. T.; Baird, G. S.; Tsien, R. Y.; Webb, W. W. *Proc Natl Acad Sci U S A* **2000**, *97*, 11996.

(65) Saffman, P. G.; Delbruck, M. *Proc Natl Acad Sci U S A* **1975**, *72*, 3111.

(66) Magde, D.; Elson, E.; Webb, W. W. *Physical Review Letters* **1972**, *29*, 705.

(67) Chen, Y.; Muller, J. D.; Ruan, Q.; Gratton, E. *Biophys J* **2002**, *82*, 133.

(68) Hur, K. H.; Mueller, J. D. *PLoS One* **2015**, *10*, e0130063.

(69) Smith, Elizabeth M.; Macdonald, Patrick J.; Chen, Y.; Mueller, Joachim D. *Biophysical Journal* **2014**, *107*, 66.

(70) Plotegher, N.; Gratton, E.; Bubacco, L. *Biochim Biophys Acta* **2014**, *1840*, 2014.

(71) Haupts, U.; Maiti, S.; Schwille, P.; Webb, W. W. *Proc Natl Acad Sci U S A* **1998**, *95*, 13573.

(72) Heikal, A. A. *Methods* **2014**, *66*, 283.

(73) Ramadurai, S.; Holt, A.; Krasnikov, V.; van den Bogaart, G.; Killian, J. A.; Poolman, B. *J Am Chem Soc* **2009**, *131*, 12650.

(74) Erickson, H. P. *Biol Proced Online* **2009**, *11*, 32.

(75) Marguet, D.; Spiliotis, E. T.; Pentcheva, T.; Lebowitz, M.; Schneck, J.; Edidin, M. *Immunity* **1999**, *11*, 231.

(76) Suhling, K.; Siegel, J.; Lanigan, P. M.; Leveque-Fort, S.; Webb, S. E.; Phillips, D.; Davis, D. M.; French, P. M. *Opt Lett* **2004**, *29*, 584.

(77) Dickson, R. M.; Cubitt, A. B.; Tsien, R. Y.; Moerner, W. E. *Nature* **1997**, *388*, 355.

(78) Widengren, J. *J R Soc Interface* **2010**, *7*, 1135.

(79) Burnette, D. T.; Sengupta, P.; Dai, Y.; Lippincott-Schwartz, J.; Kachar, B. *Proc Natl Acad Sci U S A* **2011**, *108*, 21081.

(80) Brazda, P.; Szekeres, T.; Bravics, B.; Toth, K.; Vamosi, G.; Nagy, L. *J Cell Sci* **2011**, *124*, 3631.

(81) Weiss, M.; Hashimoto, H.; Nilsson, T. *Biophys J* **2003**, *84*, 4043.

Appendix A: Thawing HEK293 Cells:

1. Warm complete media (EMEM+10%FBS+Penicillin/Streptomycin) to 37 °C.
2. Sterilize biological safety cabinet with 70% ethanol.
3. Obtain cryo-tube from -120 °C Dewar in Johnson Lab, rack 5, labeled HEK293 Cells.
4. In biological safety cabinet, warm cryo-tube in hands by rubbing it between the palms of your hands.
5. Once the frozen cells have loosened, empty contents into 50 mL conical tube containing 4.5 mL of warm complete media.
6. Pipette media to suspend cells and melt remaining cell pellet.
7. Transfer cell suspension to 25 cm^2 culturing flask with vented top. Label and place in humidified, 37 °C, 5% CO_2 incubator overnight.
8. After cells have adhered, replace media with new complete media.

Appendix B: Sub-culturing HEK293 Cells

9. Warm complete media and 0.05% trypsin-EDTA solutions to 37 °C.
10. Sterilize biological safety cabinet along with all equipment with 70% ethanol.
11. Remove flask of cell from incubator, sterilize with 70% ethanol and place in cabinet.
12. Carefully remove cap and draw up media in flask using pipet.
13. For T-25 flask add 1 mL of 0.05% trypsin-EDTA making sure to cover the bottom. Put cap back on and place in incubator for 10 min or until cells have detached from surface. If cells haven't detached after 10 min, hit the side of the flask with a firm open hand.
14. In the safety cabinet, place 4mL of complete media into flask to stop trypsinization.
15. Pipet up and down many times (~30) to break up any remaining clumps of cells.
16. Place a small aliquot of cell suspension in a micro centrifuge tube for counting (appendix C).
17. Seed new T-25 flask with appropriate cell density and pipet up and down to uniformly distribute cells.
18. Label flask with cell line, passage number, initials and date. Then place in incubator.

Appendix C: Counting HEK293 Cells

1. Combine 20 µL of cell suspension with 20 µL of trypan-blue solution.
2. Thoroughly mix and pipet 20 µL between glass coverslip and hemocytometer.
3. Using the four large quadrants of the hemocytometer, count the cells in I + II and III + IV. Then average the two values together, this is your average cell count.
4. (Avg cell count)*(10^4 cells/mL)*(total volume of suspension) = X cells
5. From here make appropriate dilutions to obtain optimal seeding density.

Appendix D: Transfection (protocol for 35 mm plates)

1. Combine 0.1-5.0 µg of DNA with 50-250 µL of warm complete media without antibiotics in 1.5 mL microcentrifuge tube.
2. Add 3.75-15 µL of Fugene HD transfection reagent to DNA-media mixture, paying close attention not to deliver volume near the walls of the container.
3. Invert tube three times and allow it to sit for 10 minutes.
4. To appropriately seeded 35 mm MatTek petri dishes, replace media with complete media without antibiotics.
5. Slowly pipet transfection media into 35 mm plates, paying close attention to evenly distribute.
6. Place 35 mm plates in a sterile, larger petri dish. Then place cell in incubator for 24-48 hours.

Appendix E: STA-200 Inhibition

1. Approximately 1 hour prior to measurements replace transfection media with 2 mL of warm media containing STA-200 (0.001 mL of STA-200 + 1.999 mL of media for 50 nM final concentration).

Appendix F: Transformation of JM109 *E. Coli* with BACE1-EGFP Construct

1. Chill sterile conical tubes on ice.
2. Obtain a microcentrifuge tube of frozen competent JM109 cells from Johnson - 80 °C
3. Pipette 50 µL of competent in a chilled tube.
4. Add 0.25 µL of BACE1-EGFP construct (Hyman Group, Johnson 4 °C, top shelf, bubble wrapped)
5. Place cell/construct mixture on ice for 10 minutes.
6. Heat shock tube in 42 °C water bath for 45 seconds
7. Chill on ice for 2 minutes.
8. Add 450 µL of cold SOC media (Johnson protocol book).
9. Incubate cells for 1 hour at 37 °C while shaking.
10. Place suspended cells and place on kanamycin agar plates using glass beads to distribute the cell suspension.
11. Incubate at 37 °C for 24 hours before picking colonies.

Appendix G: BACE1-EGFP Plasmid Prep

1. The day before plasmid prep, inoculate 5 mL of LB containing kanamycin with JM109 bacteria containing BACE1-EGFP plasmid.
2. The next day, pellet 5 mL of overnight culture by centrifuging >8000 rpm for 3 minutes.
1. Using Plasmid Miniprep kit:
2. Resuspend pelleted cells with 250 µL of resuspension buffer (Qiagen: Buffer P1) and thoroughly mix. Transfer to microcentrifuge tubes.
3. Add 250 µL of lysis buffer (Qiagen: Buffer P2) and invert tube 6 times. Do not let lysis reaction go longer than 5 minutes.
4. Add 350 µL of neutralization buffer (Qiagen: Buffer N3) and mix by inverting the tube 6 times.
5. Centrifuge tube at 13,000 rpm (all remaining centrifugations are at this speed) for 10 minutes.
6. Decant supernatant to column (Qiagen: QIAprep spin column) and centrifuge for 1 minute, discard flow-through. *For endA+ strains:* Add 500 µL of wash buffer (Qiagen: Buffer PB) and discard flow-through.
7. Wash column with 750 µL of wash buffer (Qiagen: Buffer PE) and centrifuge for 60 seconds. Discard flow-through, spin again and discard flow-through a second time.

8. Place column in clean microcentrifuge tube and place 50 µL of buffer (10 mM Tris-Cl, pH 8.5) in the center of the column, wait for 1 minute, then centrifuge for 1 minute to elute BACE1-EGFP construct.
9. Evaluate DNA concentration using nanodrop.

Appendix H: Error and Statistical Analysis

For comparing two groups

1. In Origin 8.1, highlight the two groups of values you are interested in testing.
2. Go to Statistics -> Hypothesis testing -> two-sample *t*-test -> open dialogue
3. Switch "Recalculate" to "Auto" and "Input Data Form" to "Raw".
4. Click ok.
5. Resulting statistics will be calculated assuming equal variance (Student *t*-test) and not assuming equal variance (Welsh's *t*-test).
6. If the *p*-value (Prob >) is <0.05 then the groups are statistically different. If the *p*-value > 0.05 than the groups are NOT statistically different.

For comparing three or more groups

7. Repeat the above steps but select One-way ANOVA under "statistics" instead of hypothesis testing.